FINAL REPORT

Vertical Emitting, Ring Geometry, Ultra-low Threshold and Ultra-high Speed Quantum Well Lasers for Optical Interconnect

Contract No. N00014-88-C-0483

DARPA Order No. 6325

Submitted to

OFFICE OF NAVAL RESEARCH

Arlington, Virginia

Submitted by

ORTEL Corporation

2015 West Chestnut Street

Alhambra, CA 91803-1542

January 1991

FINAL REPORT

DARPA Order No.	:	6325
Contractor	:	Ortel Corporation
Contract No.	:	N00014-88-C-0483
Contract Amount	:	$708,516.00
Effective Date of Contract	:	18 July 1988
Expiration Date of Contract	:	31 December 1990
Principal Investigator	:	Dr. Michael Mittelstein (current) Dr. Nadav Bar-Chaim (initially)
Telephone No.	:	(818) 281-3636
Title of Work	:	"Vertical Emitting, Ring Geometry, Ultra-low Threshold and Ultra-high Speed Quantum Well Lasers for Optical Interconnect"
Reporting Period	:	July 1988 - December 1990

TABLE OF CONTENT

continue TABLE OF CONTENT

continue TABLE OF CONTENT

continue TABLE OF CONTENT

continue TABLE OF CONTENT

0 PREFACE

The following constitutes the final report for work done on Contract No. N00014-88-C-0483 entitled "Vertical Emitting, Ring Geometry, Ultra-low Threshold and Ultra-high Speed Quantum Well Lasers for Optical Interconnect" during the period 18 July 1988 through 31 December 1990.

The main emphasis for this contract was placed on the efforts as highlighted in the chapter captions:

1) Introduction to optical interconnects
2) Conventional laser
3) Design of laser structures
4) Achieving buried ring structures
5) Buried ring quantum well structure
6) Buried lasers: Champion results and reproducibility
7) Ridge wave-guide laser fabrication
8) Grating fabrication
9) Grating fabrication facility
10) Test station
11) Material investigation

Every chapter starts with a brief statement to describe how it fits into the total research and development effort. An abstract is provided as section number 0 to give the content of the

chapter. References are provided in some chapters; when they apply for other chapters as well, no effort was made to repeat them. Figures are numbered with the chapter as the first digit for faster reference and a list of figure captions is provided at the end of this report as chapter 12.

This contract has supported a conference presentation (Michael Mittelstein, Israel Ury, Nadav Bar-Chaim, Kam Yin Lau, Jeffrey Ungar, and Amnon Yariv, "Ultra low threshold quantum well lasers for computer interconnects", SPIE OE/Fiber '89, Symposium on optical interconnects in the computer environment, 7. Sep. 1989, Boston Massachusetts and SPIE Proceedings, Vol. 1178, pp 177-187), a technical paper (Nadav Bar-Chaim, Kam Y. Lau, M.A. Mazed, Michael Mittelstein, Se Oh, Jeffrey E. Ungar, and Israel Ury, "Half-Ring Geometry Quantum-Well GaAlAs Lasers", Appl. Phys. Lett., Vol. 57, No. 10, pp. 966-967, Sep. 1990), and a DoD conference presentation (Nadav Bar-Chaim, Michael Mittelstein, Jeffrey E. Ungar, and Israel Ury, "Vertical emitting, ring geometry, quantum well lasers for optical interconnetions", DoD Fiber Optics Conference '90, McLean, Virginia, Mar.20-23. 1990).

1 INTRODUCTION TO OPTICAL INTERCONNECTS

After the definition of optical interconnects is given the semiconductor laser as a light source is characterized and the proposed ring laser structure - the subject of this research and development effort - is introduced.

1.0 Abstract

The benefits of optical interconnects are presented and the attractions the semiconductor laser provides are stated. The kind of laser resonator structures that are favorable for opto-electronic integration are introduced and the requirements and consequences of the proposed design are discussed.

1.1 Why Optical Interconnects

Optical interconnects are extensively used for long distance communication and are proposed for short distance interconnect as well. The short distance interconnect scheme is considered for intra computer and network application in which high to very high rates of data are to be transferred with very low bit error rates (**Figure 11**). The **conventional electrical interconnects** have been improved significantly over the last few decades, but very **high speed links** suffer from **interference** problems and from very **lossy transmission lines.**

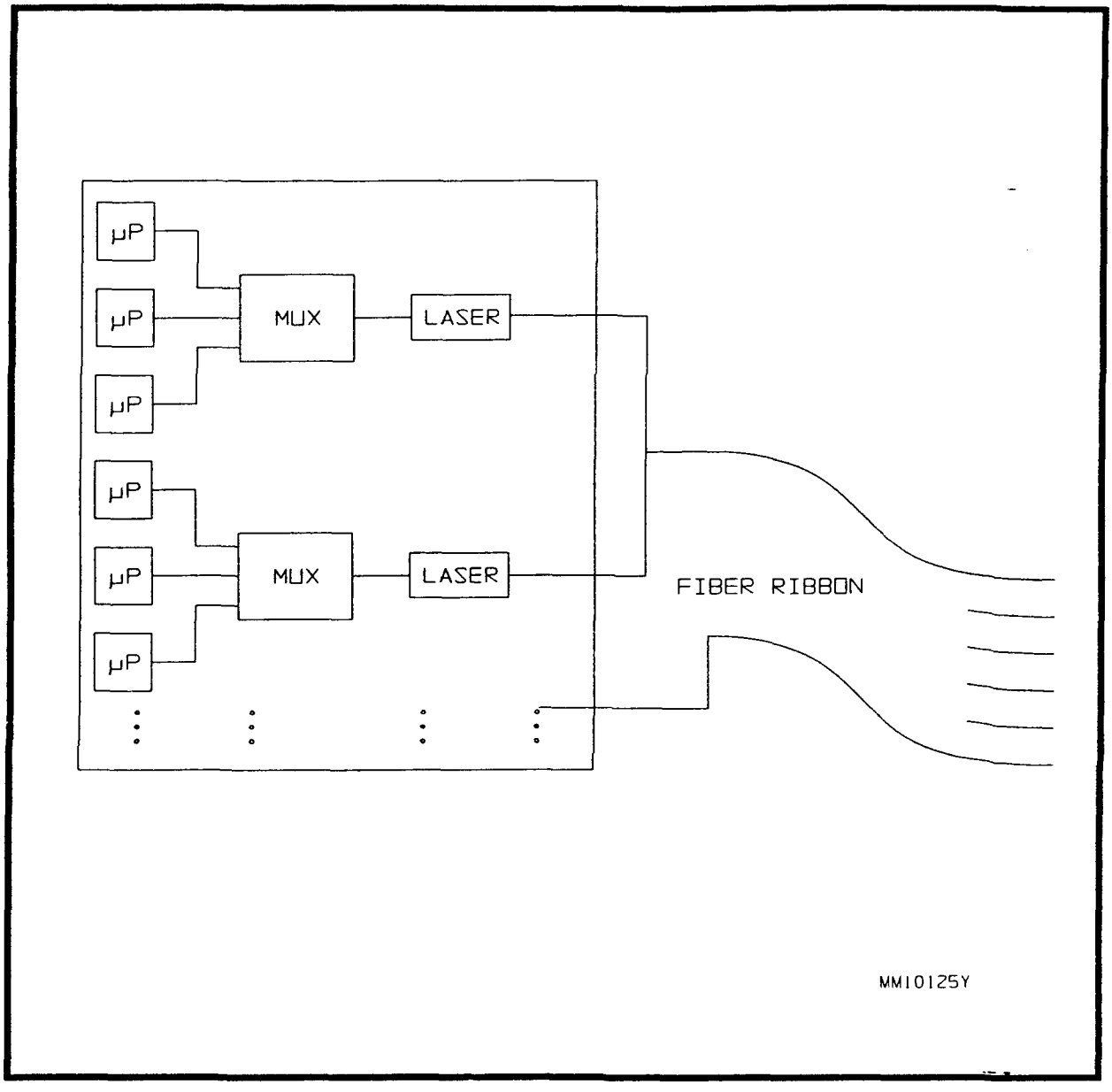

Fig. 11 Concept of implementing optical interconnects in intra computer and network application.

Optical interconnects need a lot of development, however, they fundamentally perform better regarding interference and low loss transmission when compared to their conventional electrical counter-part.

Optical interconnects for communication purposes require a **light source** capable of modulating the information to be transmitted on the output light, a **channel to transmit the modulated light,** and a **light receiver** capable of resolving the modulation and therefore the information sent through the interconnect. The channel, which is the main problem in conventional electrical interconnects, can be as simple as free space in the case of the optical interconnect. The advantage of the optical interconnect is the near absence of interference; for instance a single lens can be the channel of 100,000 parallel links (the arrangement would be like in a projection-TV-set). Other options include two dimensional optical wave-guide structures fabricated with planar photolithographic technology and more conventional single mode fibers as a point to point channel.

At this point in the research and development the light source seams to be the component that requires the largest effort. For high speed interconnects the semiconductor laser is an extremely attractive light source. **Semiconductor injection lasers** can be modulated at 10 GHz and beyond by direct **drive current modulation.** They are **physically tiny** and being all

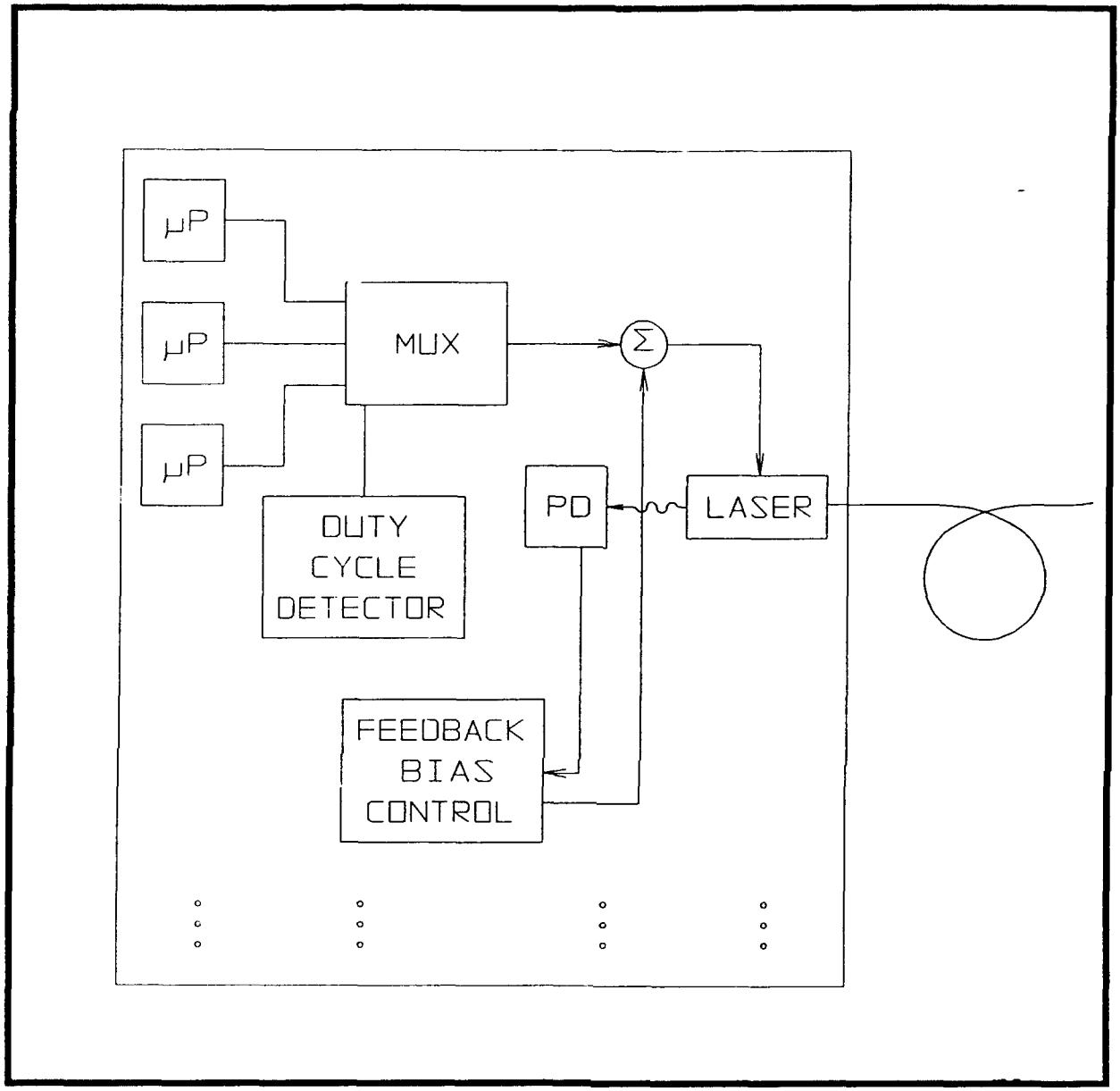

Fig. 12 Detail of monitor photo diode (PD), Feedback Bias Control, Duty Cycle Detector, and Current Summing ($\sum$) components required for proper operation of conventional semiconductor laser operation in an optical interconnect. This complexity stimulates considerations about direct drive no lasing bias operations of optical interconnect lasers.

solid state relatively rugged. They are one of the highest efficiency light sources available and their direct modulation capability at voltages near 2 Volts and moderate currents allow to integrate them with high speed electronics easily. Continued efforts will provide no laser bias direct drive operation as indicated in Figure 12 (see section 2.6 for explanation). Work for this contract concentrates on research and development of lasers for optical interconnects.

1.2 Integrated Semiconductor Laser

Individual semiconductor injection lasers for optical interconnects have been developed for quite some time now. We describe an investigations of conventional double cleaved lasers in chapter two with a near term future projection and evaluation of that type of device and its performance estimates. However, for compact high speed network or computer systems of the future high density monolithic integrated optical interconnects are preferable. Semiconductor material of GaAs/GaAlAs composition is already used for high speed electronics and this material combination is proven for opto-electronic devices. Consequently it provides a favorable material system to proceed with the development of laser emitters for optical interconnects.

Very large scale opto-electronic integration includes the challenge of multiple lasers on a single ship. This is the key

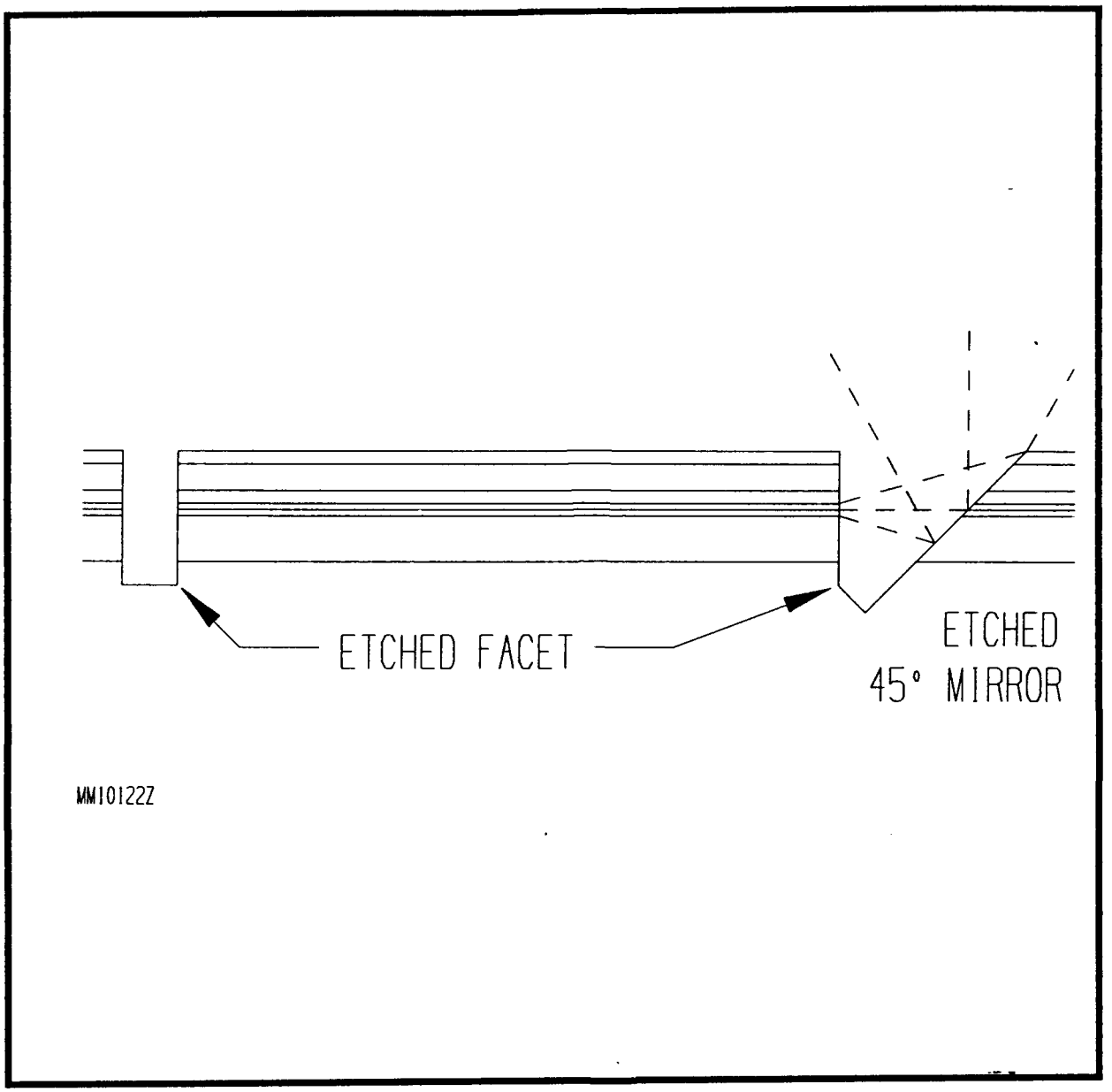

Fig. 13 Concept of implementation of extra cavity folding mirror in a monolithic vertical emitting laser.

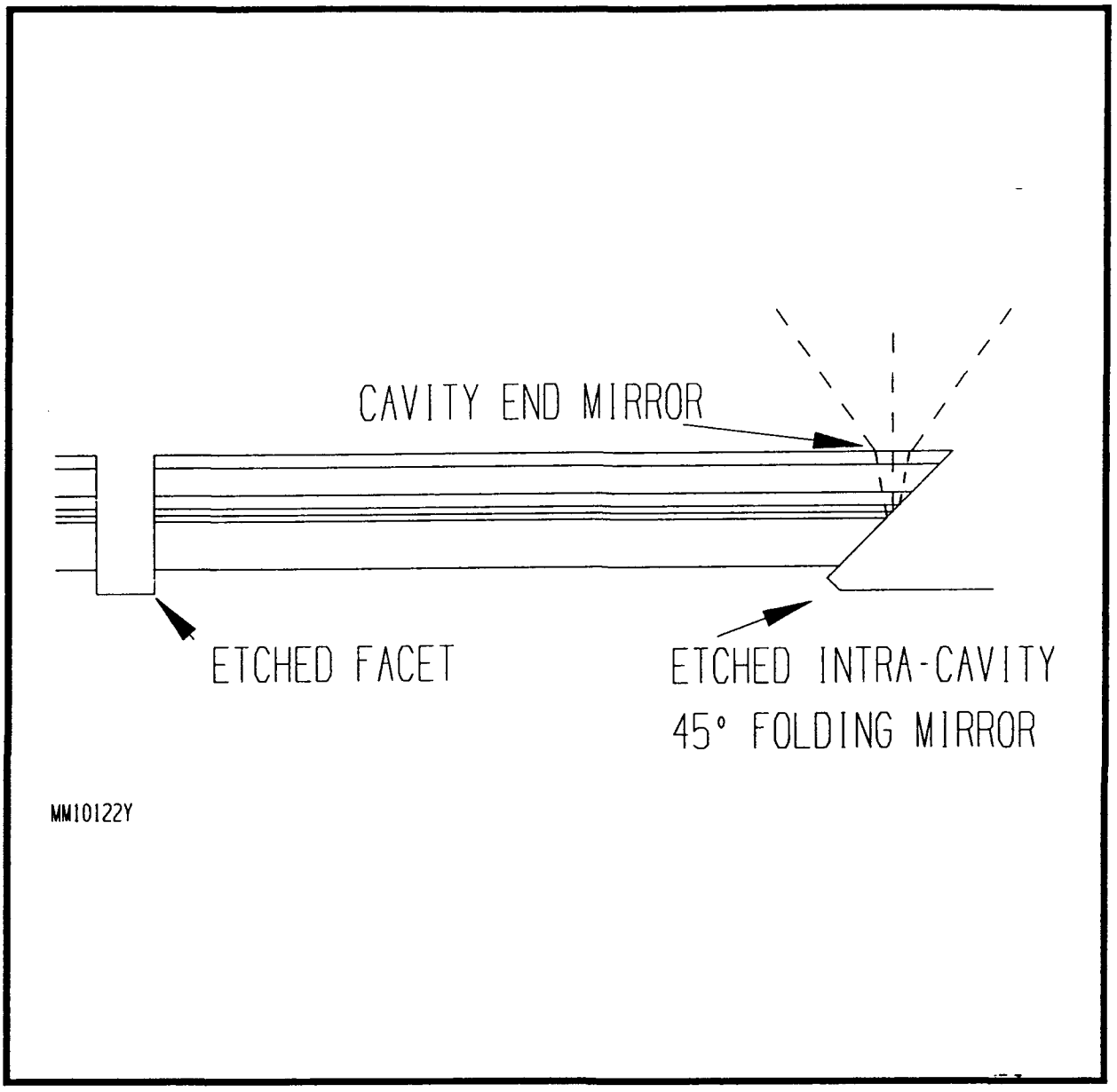

Fig. 14 Concept of implementation of intra cavity folding mirror in a monolithic vertical emitting laser.

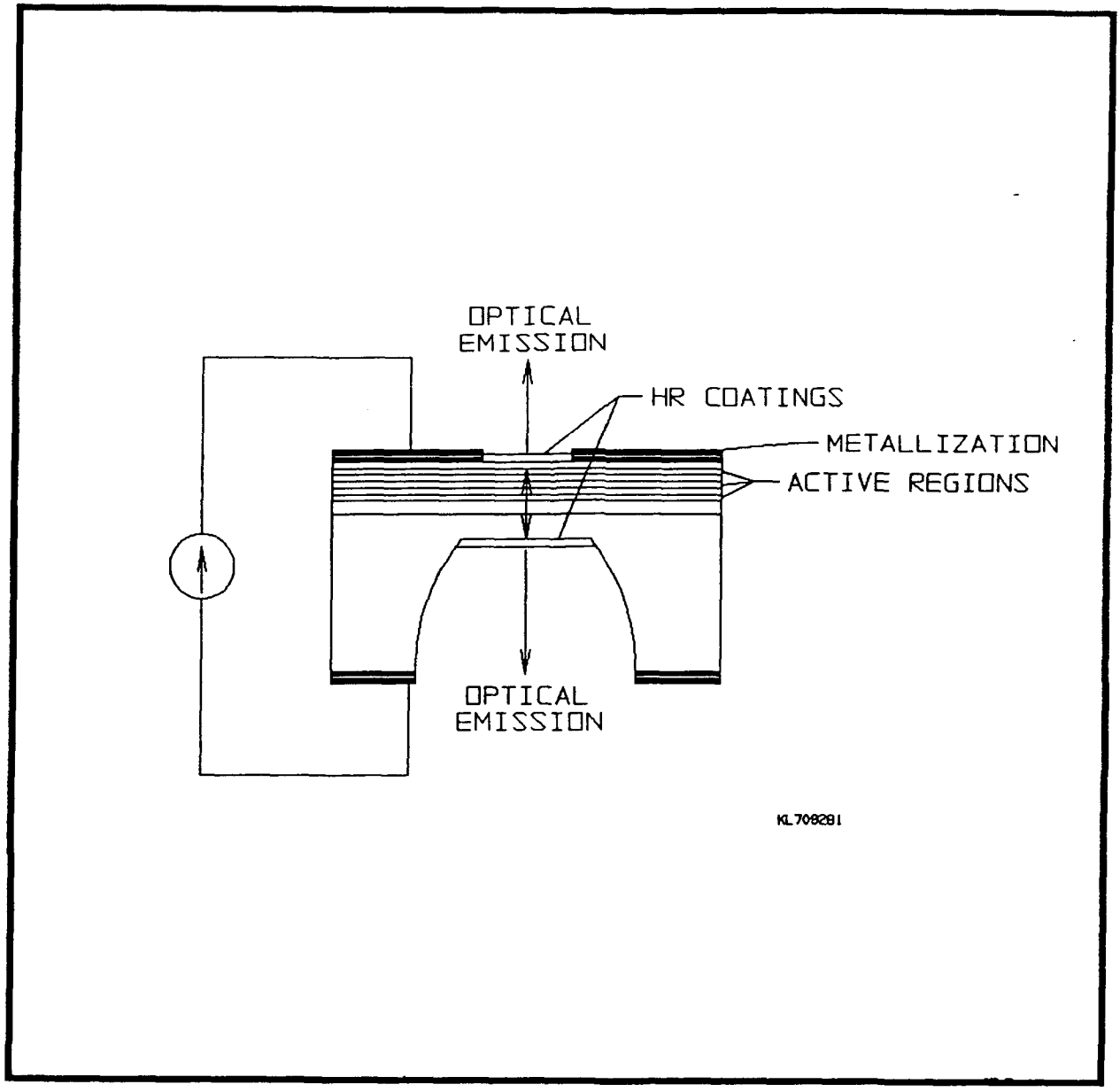

Fig. 15 Vertical short cavity, vertically emitting laser utilizing multiple active regions here shown with conventional mirrors.

development necessary for reaching high density integration. Utilizing the conventional double cleaved semiconductor laser puts a severe **constraint on one dimension** of the opto-electronic chip. The optimum resonator length of integrated lasers for high speed optical interconnect depends on the laser structure utilized, but is probably in the 100 µm to 300 µm range. This small size and the electrical interconnect restrictions exclude the conventional double cleaved laser from large scale opto-electronic integration. Alternatives to implementing a conventional resonator include etched facets and mirco-cleaving both of which have not shown good reproducibility or reliability so far. Such methods can be used to produce the back facet of a laser whose output facet is the etch of the chip. More advanced schemes utilize **mirrors to redirect** the light so that a vertical emission is accomplished as shown in **Figure 13** and **Figure 14**. Another arrangement is to implement the **cavity in the vertical direction**, an approach which showed promising results very recently (**Figure 15**). However, an other alternative is provided by curved resonator configurations.

1.3 Curved Resonators

The resonator structures mentioned in the previous section use a straight active region for the gain of the laser. This constitutes a restriction that is not necessary. If a narrow stripe optical wave-guide is implemented, which depends on real

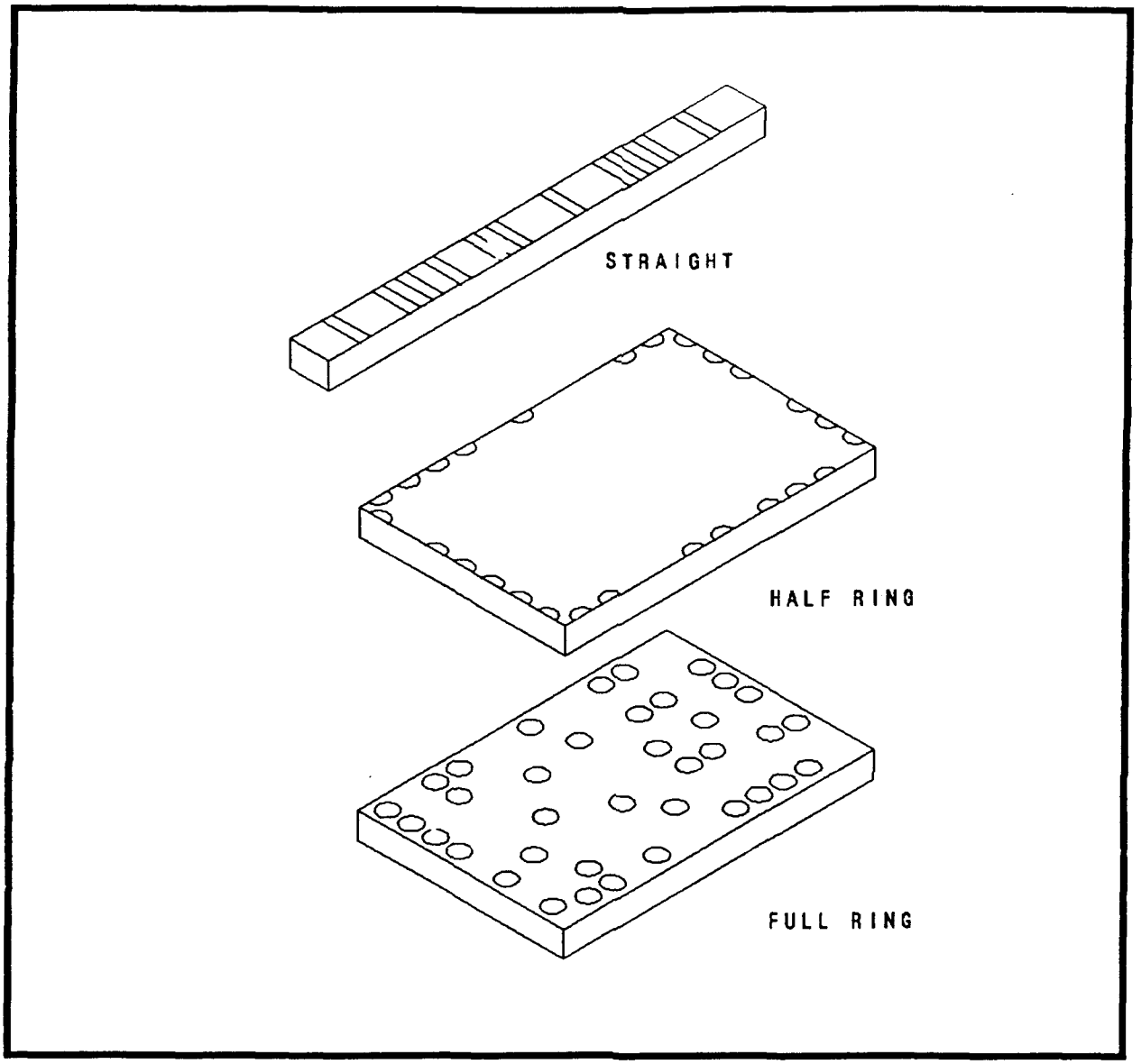

Fig. 16 Conventional double cleaved lasers (top) half ring lasers (middle) and full ring lasers (bottom) integrated in a large scale integrated opto-electronic circuit. Not the restriction on the chip size due to the resonator size in the conventional case. In the case of full ring lasers all restrictions on the placement of the lasers within the integrated circuit have been removed.

index guiding, than a curtain amount of **curvature of the guide** is tolerable. The guiding properties can be maintained down to a radius of curvature at which the additional losses became unacceptable. **Resonators** utilizing curved active regions can be implemented with **new properties (Figure 16).** For instance the **requirement of a second facet can be eliminated** by introducing a 180° turn in the wave-guide such that both ends of the resonator point to the same side and utilize the same facet. Consequently lasers for optical interconnects could be lined up along the periphery of the chip and therefore do not restrict the dimension of the opto-electronic integrated circuit. Furthermore, a 360° turn allows closing the resonator structure to a **ring resonator all within the semiconductor chip.** In the latter case a new output coupling scheme has to be added since the laser is **facetless.** However the laser can be placed anywhere on the chip. This provides a tremendous degree of added **freedom in positioning** and therefore designing a highly integrated opto-electronic circuit and makes the design rules for integrating these laser similar to the rules used for the majority of the other components in the integration. This are not the only possible resonator configurations for optical interconnects, rather they are what this research and development effort is concentrated on.

2 CONVENTIONAL LASER

An evaluation of the state of the art of lasers was performed in the summer of 1989 and a projection for the application of computer interconnects was published as a presentation ''Ultra low threshold quantum well lasers for computer interconnects'' at the SPIE OE/Fiber '89.[0] This chapter also serves as an introduction to the state of the art technology, which has been updated in the appendix of this chapter.

2.0 Abstract

Optical computer interconnects appear very attractive when integration of state of the art technology of quantum well GaAs/GaAlAs lasers is considered. These ultralow threshold lasers provide the very high transmission rates and the inherent simplicity required for such systems. A detailed design is presented for a 5 Gbit s^{-1} transmission rate, suppression of pattern effects, and a system power supply of approximately 25 mW per laser. Existing experimental data show that little extrapolation is required to reach that kind of performance from state of the art technology.

2.1 Introduction

The replacement of electrical interconnects with optical interconnects for board-to-board communications will necessitate a **large number of optical emitters** and detectors[1]. It is estimated that a typical supercomputer will require as many as 10^5 emitter/detector pairs.

Conventional semiconductor lasers, having threshold currents of 20 mA or so, fall short of meeting the requirements for these interconnects for two reasons[2]. First, these lasers must be prebiased to the lasing state in order to achieve high speed switching operation. This continuous current flow leads to excessive power dissipation in the computer. Secondly, and more importantly, the required bias current varies from device to device, over the life of the device, and over temperature. The conventional approach of sampling the emission from the rear facet of the laser and applying this signal as feedback to a bias current controller is too cumbersome in terms of size, complexity, and cost.

The use of **ultralow threshold current lasers** substantially eliminates both of the above mentioned objections to the use of lasers[2]. The ultralow threshold current laser does not require prebiasing to achieve fast turn-on because they can be

driven with current pulses exceeding threshold by significantly more than a factor of ten. Without prebiasing power dissipation is reduced and feedback circuitry is eliminated.

Single quantum well buried heterostructure (**SQW BH**) lasers having threshold currents as low as 0.55 mA have been fabricated[3]. The SQW structures were grown by molecular beam epitaxy (**MBE**), and more recently by metal-organic-chemical vapor deposition (**MOCVD**). The SQW active layer material displays much **lower transparency current densities** than conventional double heterostructure material that have a much thicker active region. The low value of the transparency current density is converted to a low value of threshold current by fabricating devices having **narrow stripe width** and **short cavities** to cut down the area of the pumped region, and **higher mirror reflectivity** to keep the required optical gain at a moderate level.

Experiments to demonstrate the high speed switching characteristics of devices without prebias have been performed[2]. Switch-on delays of less than 70 ps have been observed with no subsequent ringing.

The following is the list of the subjects to be discussed in this chapter:

2) Why Quantum Well Lasers

3) Performance of Single Quantum Well Structures

4) Scaling the Size for Communication Lasers

5) Experimental Findings to Date

6) Projected Performance Figures

7) Alternate Schemes for Vertical Coupling

8) Future Improvements

2.2 Why Quantum Well Lasers

The benefits of quantum well lasers over conventional double heterostructure lasers have been investigated (e.g. Ref. 4). Fundamentally, the double heterostructure is capable of producing high optical gain; in nearly all applications, this capability is not taken advantage of[5]. By carefully optimizing the structure to provide the **moderate amount of gain actually used**, the design ends up with a very **small thickness of the active region.** Devices with very thin active regions (<200 Å for room temperature operation) show quantum effects and are therefore called **quantum well lasers.** In most applications, the quantum structure effects are not the major benefit; the sheer small size of the active region is what is taken advantage of. Because the gain produced by quantum well lasers is moderate, careful attention has to be paid to the design of the optical

cavity[6,7]. The major benefit of suitably designed quantum well lasers is reduced threshold current density with respect to conventional double heterostructure lasers.

Experimentally, it is found that with respect to internal quantum efficiency and distributed losses, laser performance is improved if the threshold current density is kept low. It is advantageous to use a low loss resonator design with a single quantum well structure rather than using a somewhat higher loss cavity with a conventional double heterostructure simply because the current density is significantly reduced. Some of the quantum characteristics provide further improvement on the basic performance gain.

2.3 Performance of Single Quantum Well Structures

If quantum well structures are used, a choice has to be made as to how many quantum wells are to be incorporated. A **multiple quantum well structure** is the structure of choice if a single quantum well structure cannot provide sufficient gain. **If the design is free to be optimized for a low threshold current laser, the gain requirement is a parameter to be determined. Therefore, the optimum choice is to operate the laser with the low gain requirement which is ideally provided by a single quantum well laser.**

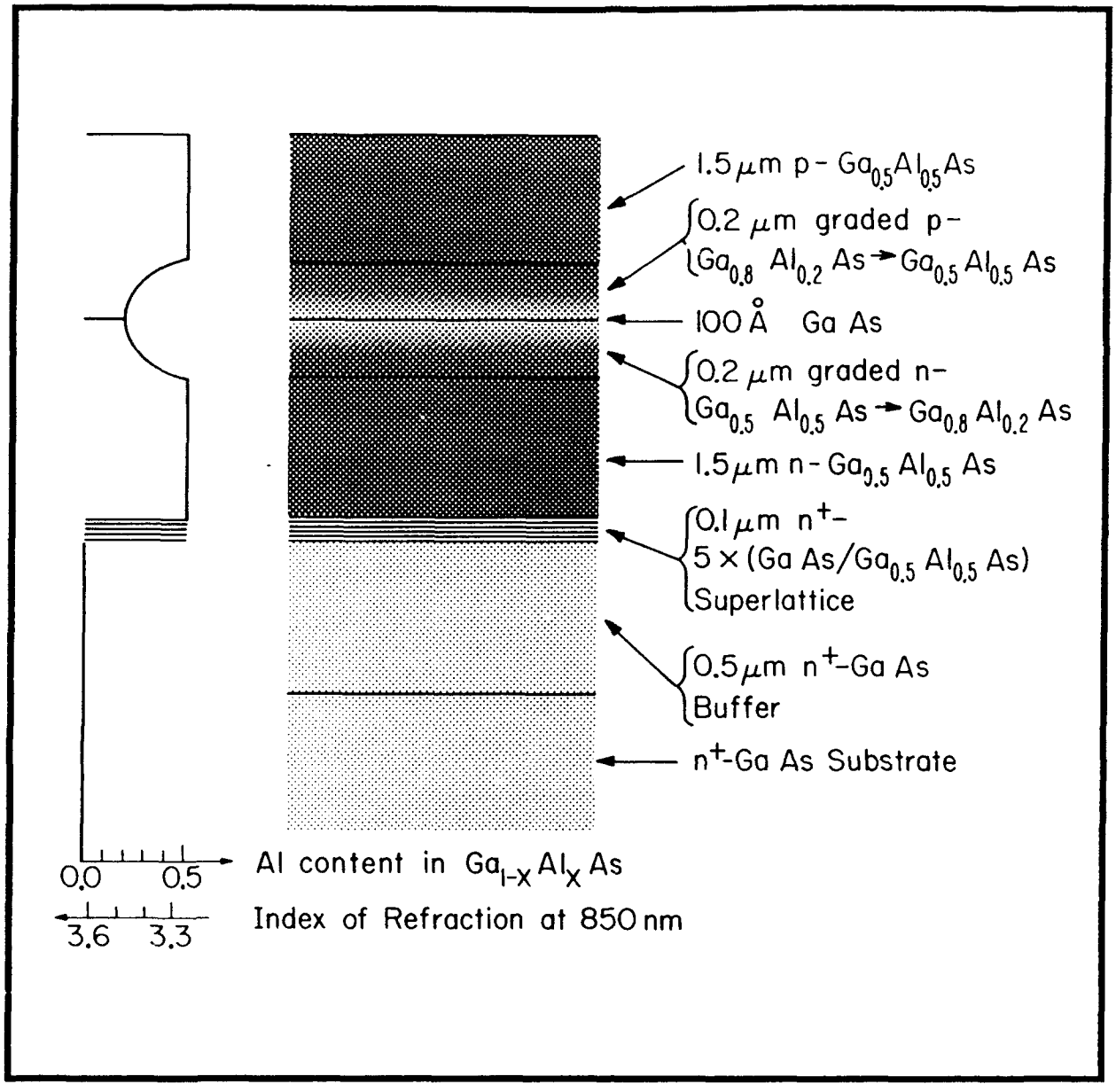

Fig. 21 Single quantum well layer structure[10]. On the left, the profile of the Al-concentration is illustrated as well as the approximate index of refraction of the material.

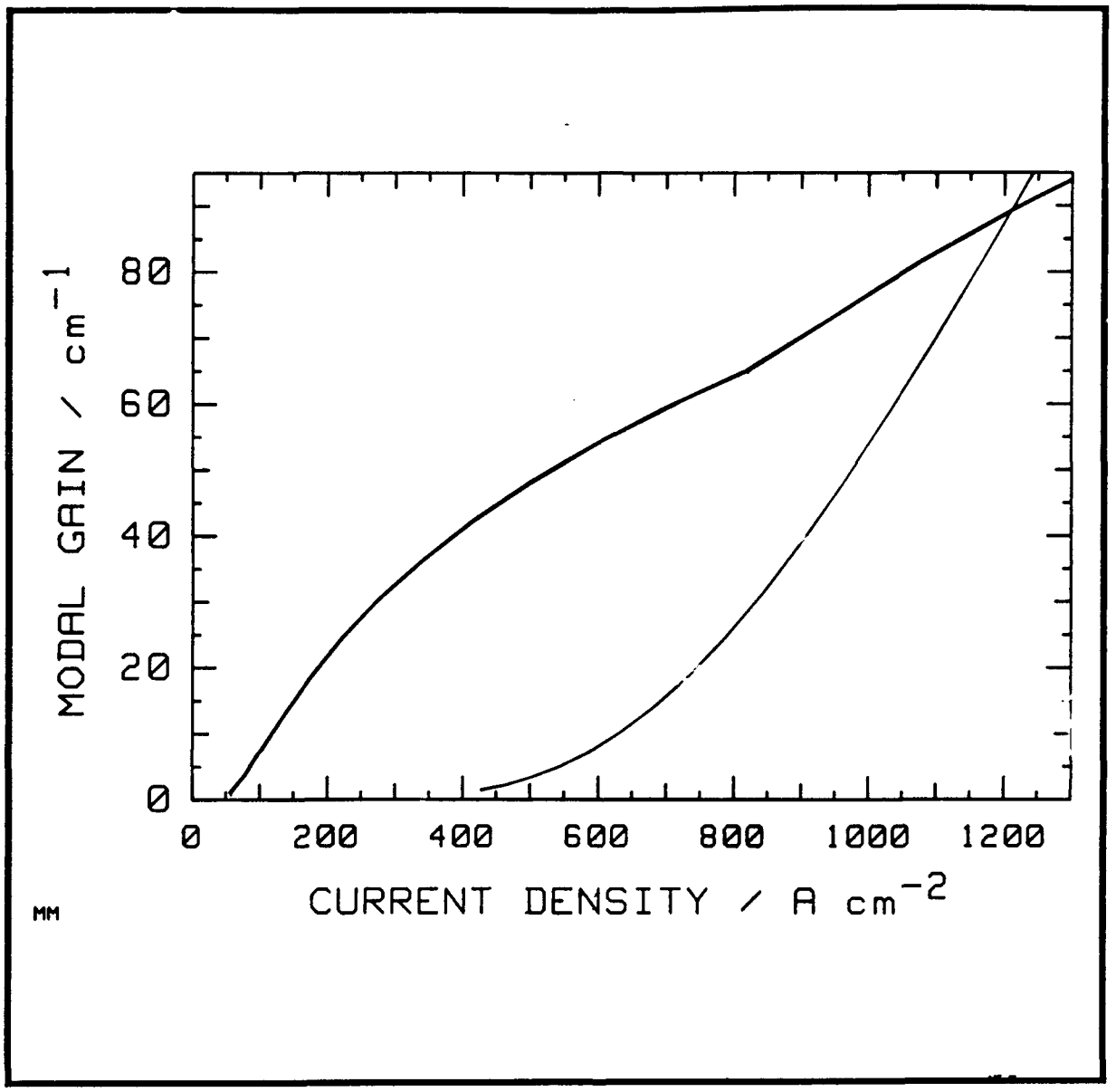

Fig. 22 Calculated modal gain vs. pump current density[5]. The upper trace applies for the single quantum well structure shown in Figure 21 the lower right trace applies to a conventional double heterostructure laser.

Single quantum well structures have been studied extensively (e.g. Ref. 8, 9). An example of the vertical structure of a "standard" single quantum well lasers is shown in **Figure 21** [10]. The structure incorporates a graded region around the quantum well to guide the optical mode. The effective width of the optical mode in this structure is approximately 3000 Å. Based on extensive calculations[5], **Figure 22** shows the **modal gain** of this structure in comparison to the double heterostructure with the same optical mode width. The significant **improvement for low modal gain** is evident.

High quality material single quantum well lasers with long resonators will exhibit threshold current densities of approximately 200 A cm^{-2}. If the gain requirement is kept low, corresponding to a modal gain around 20 cm^{-1} to 30 cm^{-1}, this current density can be maintained even in shorter cavities. **The requirement is then to increase the reflectivites such that the output coupling, when considered as a distributed loss, is kept constant.** This is the preferred operational condition for a short cavity single quantum well laser.

For a conventional double heterostructure, the calculated **modal gain to current density ratio** is monotonically increasing for modal gains of up to 100 cm^{-1} and beyond (**Figure 22**). For

single quantum well lasers a maximum is reached near 30 cm^{-1} of modal gain, at a current density so low that the conventional laser cannot produce any gain.

The dependence of modal gain on current density is the main distinguishing feature of the two structures. Experimentally, it is found that the calculated values of modal gain are too optimistic for current densities higher than 500 A cm^{-2}. This leads to a pronounced flattening of the available modal gain at high pump current densities. Resonator designs which require low modal gain are clearly desirable.

Quantum well lasers benefit from two more properties of the quantum well structure. The **internal quantum efficiency** of these structures has been found to be superior to double heterostructures. Reproducible values close to **90%** have been measured [9,11,12]. Secondly, the **distributed losses** of single quantum well structures are the lowest of all semi-conductor lasers. These low internal losses lead to higher output efficiencies even if the low output coupling is selected.

2.4 Scaling the Size of a Communication Laser

For short distant communication, as in a computer, the optical losses of the communication link can be expected to be moderate. Therefore, no premium has to be placed on the **absolute output**

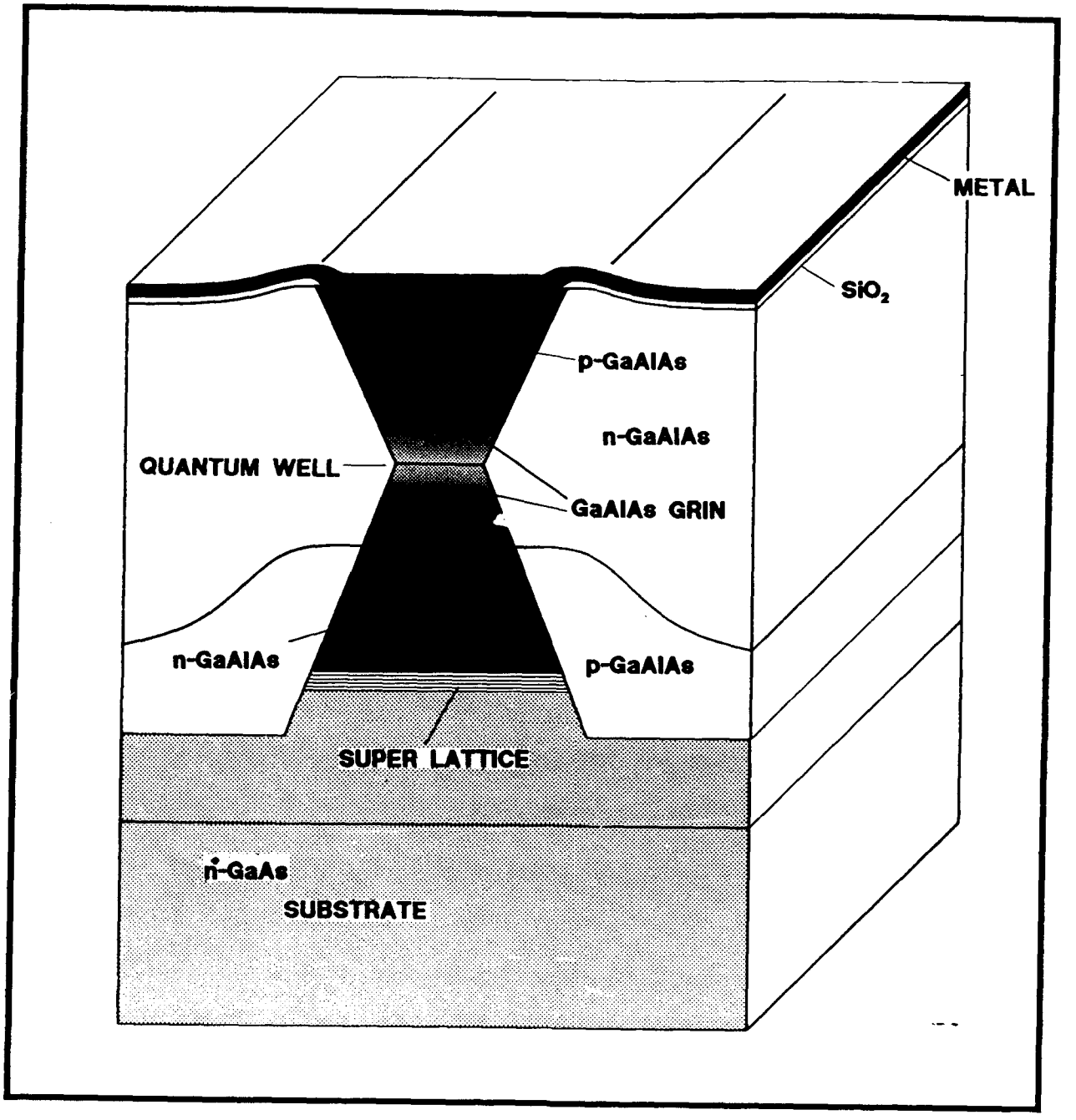

Fig. 23 Structure of the buried heterostructure single quantum well laser.

power of the emitting laser. Consequently, lasers as small as possible are advisable. Scaling the size of the laser down reduces the total threshold current.

Assuming the vertical structure is not changed and remains as shown in **Figure 21**, the widths and lengths of the laser can be scaled. Proven technology allows to scale the widths down to 1 μm . Typically the buried heterostructure design is used for such narrow lasers (**Figure 23**). At about 1 μm width of the active region, typically an optical mode width close to twice as wide as the active region is to be expected. This has two consequences. The modal gain as provided by the quantum well is reduced to nearly one half, and the buried structure typically also exhibits increased distributed losses. Measured values indicate 10 cm^{-1} or lower. This puts a constraint on the scaling for the lengths of the laser unless we consider extremely high reflectivities.

A good high reflectivity coating can provide **0.95 reflection**. If the device is made asymmetric to emit most of the light on one side as it is advantages for optical communication, that side should have a lower reflectivity. For example, an **output reflectivity of 0.83** results in **cavity lengths** of approximate **120** μm to meet the above introduced criteria.

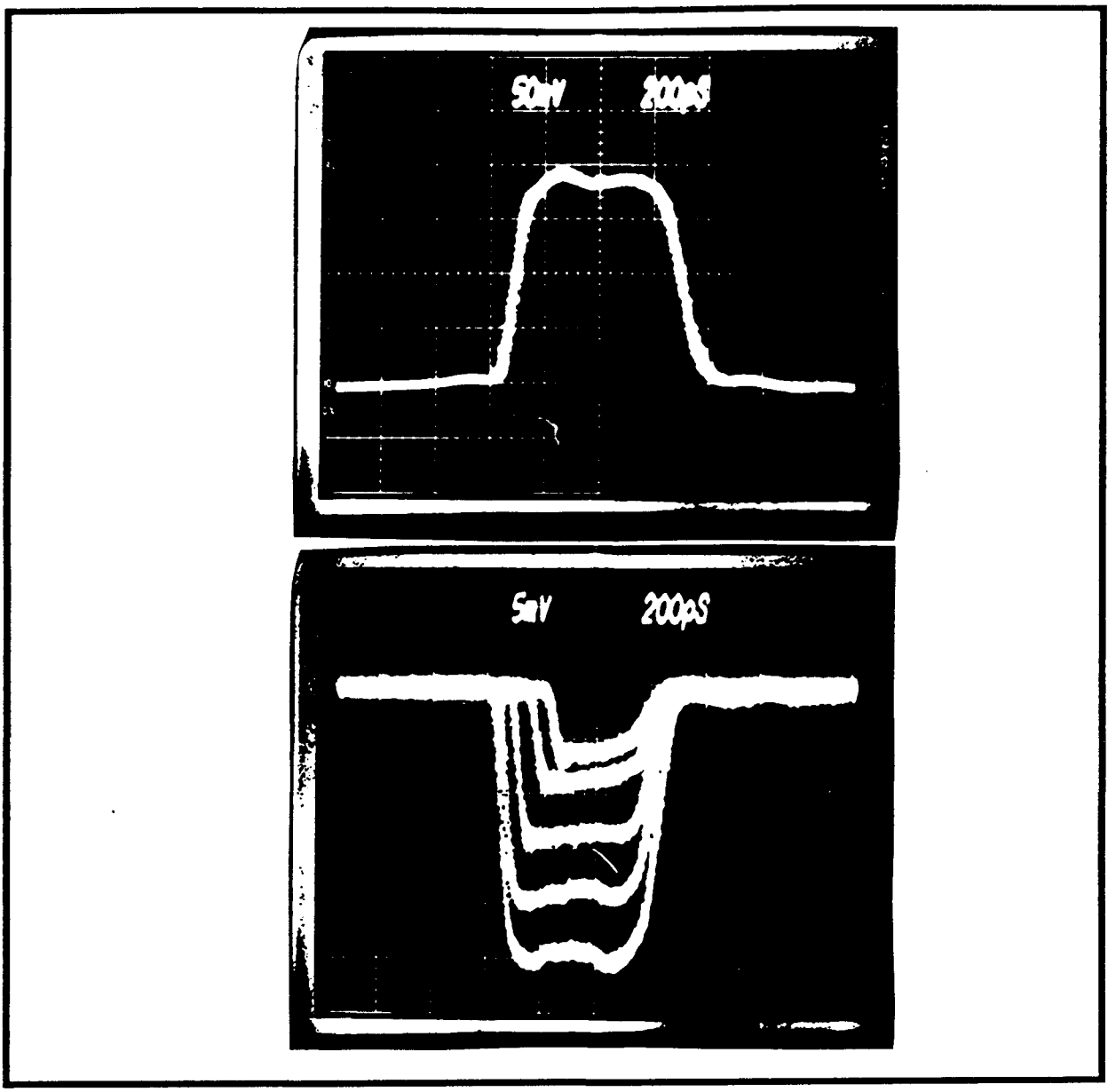

Fig. 24 Pulse response of 0.95 mA threshold quantum well laser. At the top a typical drive current pulse. At the bottom (inverted scale) light output response at peak currents of 7.4, 10.8, 16.8, 23 and 30 mA ^{2}.

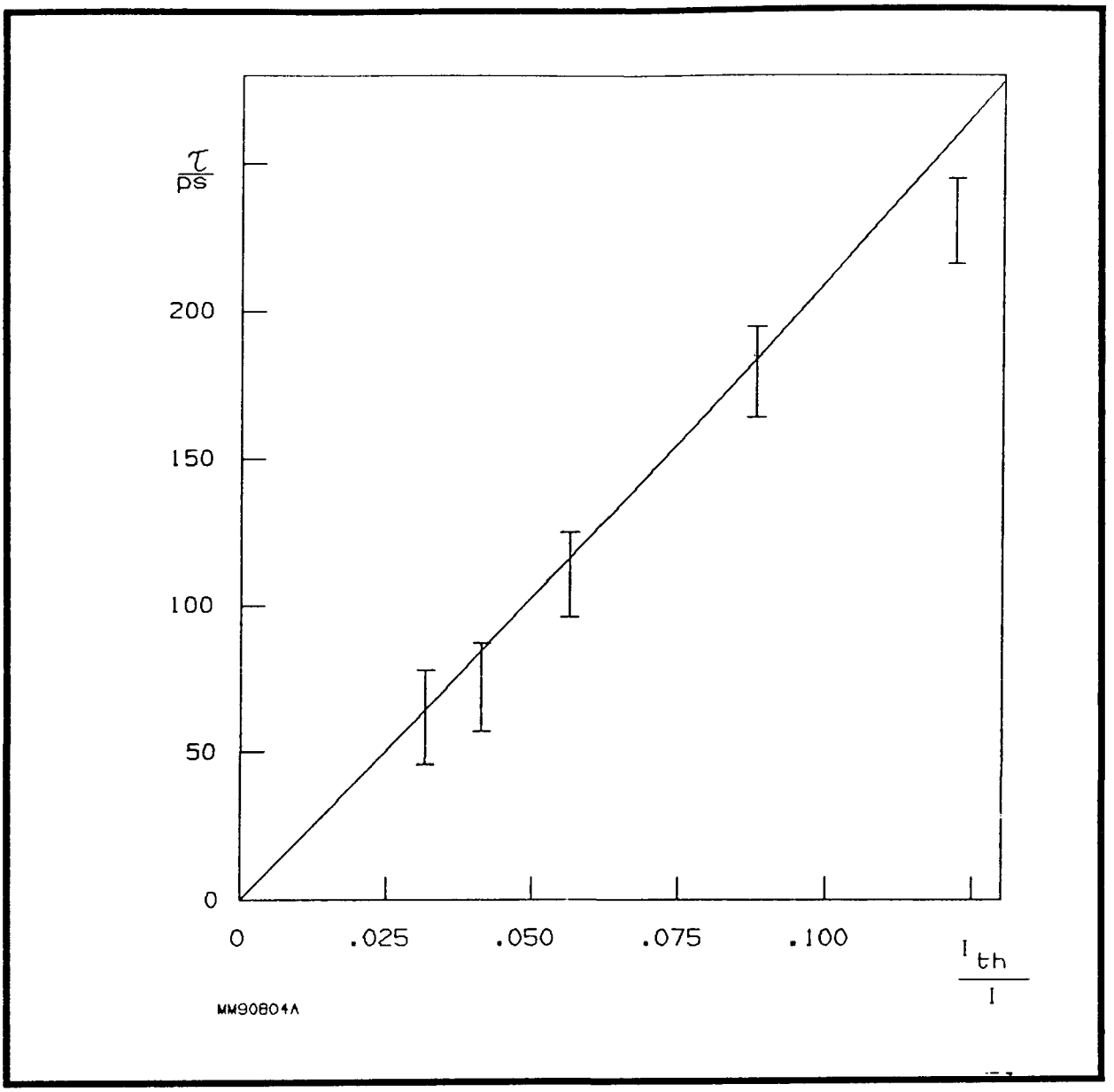

Fig. 25 Measured delay of laser output light in response to drive current pulse as a function of threshold to pulse current ratio. The absolute time reference for the delay measurement is obtained by fitting to a calculation based on a 2 ns average lifetime of the carriers at threshold.

2.5 Experimental Findings to Date

For the experiments, a structure as shown in **Figure 21** was optimized for liquid phase epitaxy regrowth to produce buried single quantum well laser structures. The quantum well structure was grown using a molecular beam epitaxy facility at the California Institute of Technology by Pamela L. Derry. Buried lasers 1 µm wide and 250 µm long were fabricated. After increasing the reflectivity to about 0.7 , those laser exhibited threshold currents as low as 0.95 mA [13] . These lasers were used in high speed digital modulation experiments where **rectangular current pulses** of different amplitude were applied to the laser **without biasing.** The resulting large signal response is shown in **Figure 24.** Note that the leading edges show delays depending on the amplitude of the current pulse, while the time of the falling edge of the light pulse seems to be independent of the amplitude of the current pulse.

A careful reevaluation of the measurement shown in **Figure 24** is shown in **Figure 25** . The problem is to find the absolute reference for the delay of the light output vs. current driving the laser. This parameter has been adjusted to obtain good **agreement with a simple model.** The model is based on an **average carrier lifetime of 2** ns **at threshold.** The delay time is calculated as the time necessary to build up the carrier density to the threshold condition. At the highest pulse current

measured (30 mA), the laser exhibits a delay of less than 70 ps in the light output in response to a current pulse. **This time is essentially the lifetime of the carriers in the laser when operating at such a "high" current[5].** The other remarkable result is the **absence of ringing.** The laser seems to follow the current pulse very closely. Most likely, this is caused by the very short average lifetime of the carriers in the laser due to high rates of stimulated emission and the nonlinear gain current relation shown in **Figure 22** resulting in significant damping.

Similar lasers have been cleaved to resonators of a length of 120 μm and coated with high reflectivity coatings to obtain 0.55 mA threshold[3]. This shows that scaling to shorter devices length using higher reflectivity coatings follows theory closely. Further evidence is obtained from measuring the slope efficiency of these devices[14]. If the distributed losses in these lasers are low, the measured slope efficiency should change little when shorter devices with higher reflectivity coatings are used. Again, the theory is in good agreement with the experiments.

2.6 Projected Performance Figures

The good agreement of measured data with theoretical predictions allows us to scale the resonator size of the laser with high confidence. The purpose is to give an example of a possible design for the implementation of a high speed short distance communication laser. This is chosen in contrast to deriving exact optimization criteria and estimating all entering parameters to find optimized values. Consider the proposed laser of 1 µm width and 120 µm length with high reflection coatings of 0.83 and 0.95 reflectivity on the output side and back side respectively. Assuming a current density of 225 A cm^{-2} at threshold, a **0.27** mA **threshold current** is predicted. If this device exhibits an internal quantum efficiency of 0.85, a total quantum efficiency at the output facet of 0.33 results and 0.5 W A^{-1} can be expected.

If an average carrier lifetime of 2.7 ns at threshold is assumed, the carrier density per area is 3.8 10^{12} cm^{-2}. If not more than 50 ps delay is required, the value for the **drive current of the laser is 15** mA to reach that carrier density starting from zero within that delay time. At 15 mA, the laser is estimated to have a resonance frequency of about 9.5 GHz. This is of secondary importance as long as the laser is driven with large modulation depth. The intended operation is pulsing the laser from below threshold to 15 mA, which presents more than

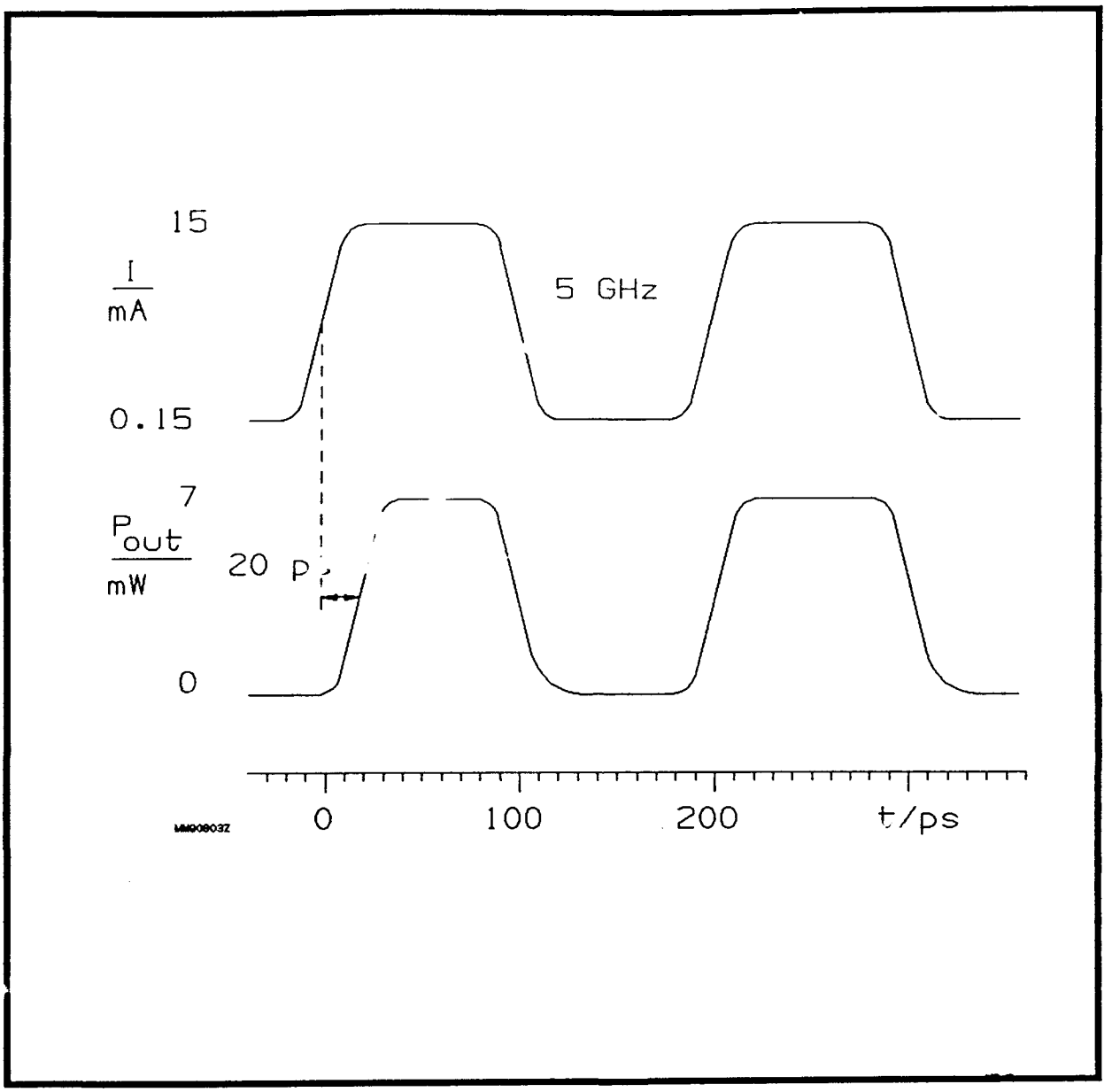

Fig. 26 Schematic of pulse response of proposed laser structure. Driven with 15 mA current pulses from an idle current of 0.15 mA (non-lasing) a pattern effect not exceeding 20 ps is expected.

50 times threshold current. Under these conditions, the actual variation in turn-on delay, known as the **pattern effect**, should be **no more than 50** ps, depending on the presence or absence of a preceding pulse. If the laser is **biased at about half the threshold current**, (it is not lasing before the pulse arrives) the pattern effect should be decreased to about **20** ps. In the schematic **Figure 26** , the response to a leading and immediately following pulse is indicated showing the full range of the pattern effect.

Assuming a duty cycle less than 0.5 for driving the laser and the use of a 3.3 V power supply, implies **below 25** mW **of average system power demand per laser.** The obtainable transmitted bit rate for this laser should be at least 5 Gbit s^{-1} .

2.7 Alternate Schemes for Vertical Coupling

In the preceding paragraphs, lasers with two facets have been considered. In the application of optical interconnects in computers, a different scheme which allows coupling light out of the laser without using facets perpendicular to the wafer surface may be preferred. Methods of applying second order grating distributed feedback lasers which provide vertical output seem promising[15,16,17]. An alternative scheme is to use an optical resonators in the vertical direction[18,19]. These

two schemes have been worked on for quite a while. They have not yet shown performance approaching the kind of performance described for lasers with conventional resonators.

2.8 Future Improvements

Future improvements are expected from two main sources. First, improvements on the vertical structure should lead to even lower threshold current densities for the same gain requirement. Improvements have already been reported on MBE material reaching **threshold current densities below 100** A cm^{-2} [20].

It has been suggested, that strained layer quantum well lasers incorporating InGaAs can improve the threshold current density one order of magnitude[21]. These structures will exhibit modified properties such as lasing wavelengths in the region near 1000 nm. This may be advantageous on one hand because GaAs and GaAlAs material is transparent at that wavelength. On the other hand, this may prove to be a problem because GaAs and GaAlAs structures cannot be used as a detector for that wavelength. Secondly, improvements could stem from new structures and geometries. Very narrow lasers have been demonstrated using patterned substrates and advanced growth methods[22]. New structures may also involve novel resonator arrangements[23]. More basic alternative may include **active regions of quantum wires or quantum dots**[5,24,25,26].

The major improvements necessary for the application of optical interconnect in computers is the development of **high yield processing techniques.** This application probably calls for highly integrated chips which carry a large number of lasers. The present yield of individual lasers is not sufficient to produce chips containing many lasers reproducibly.

2.9 Summary

Optical computer interconnects appear very attractive. Single quantum well lasers exhibit properties leading them to become a prime candidate for high speed communications in this application. For short distance links, there is no requirement for high output power. Optimized structures are, therefore, scaled down to lasers of very small size. Experimental findings to date give threshold currents as low as 0.55 mA. Test lasers indicate that scaling laws can be applied with high confidence. A laser designed with a threshold current of 0.27 mA is discussed leading to a 5 Gbit s^{-1} transmission rate with a system power supply requirement of only 25 mW per laser.

2.10 References

0. Michael Mittelstein, Israel Ury, Nadav Bar-Chaim, Kam-Yin Lau, Jeffrey Ungar, and Amnon Yariv, "Ultra low threshold quantum well lasers for computer interconnects", SPIE OE/Fiber '89, Symposium on optical interconnects in the computer environment 7. Sep. 1989, Boston Massachusetts and SPIE Proceedings, Vol. 1178, pp 177-187.

1. J.W. Goodman, F.Y. Leonberger, S. Y. Kung, and R. A. Athale, "Optical Interconnections for VLSI systems", Proc. IEEE, Vol. 72, pp. 850-864, 1984.

2. K. Y. Lau, N. Bar-Chaim, P.L. Derry, and A. Yariv, "High Speed Digital Modulation of Ultralow Threshold (<1 mA) GaAs Single Quantum Well Laser Without Bias", Appl. Phys. Lett., Vol. 51, No. 2, pp. 69-71, 1987.

3. K. Y. Lau, P.L. Derry, and A. Yariv, "Ultimate Limit in Low Threshold Quantum Well GaAlAs Semiconductor Lasers", Appl. Phys. Lett., Vol. 52, No. 2, pp. 88-90, 1988.

4. Y. Arakawa, and A. Yariv, "Theory of Gain, Modulation Response and Spectral Linewidth in AlGaAs Quantum Well Lasers", IEEE J. Quant. Elect., Vol. QE-21, pp. 1666-1674, 1985.

5. Michael Mittelstein, "Theory and Experiments on Unstable-Resonator and Quantum-Well GaAs/GaAlAs Lasers", Ph.D. Thesis, California Institute of Technology, Pasadena, CA, March 1989.

6. P. S. Zory, A. R. Reisinger, L. J. Mawst, G. Costrini, C. A. Zmudzinski, M. A. Emanuel, M. E. Givens, and I. J. Coleman, "Anomalous Length Dependence of Threshold for Thin Quantum-Well AlGaAs Diode Lasers", Appl. Phys. Lett., Vol. 49, No. 1, pp. 16-18, 1986.

7. M. Mittelstein, Y. Arakawa, A. Larsson, and A. Yariv, "Second Quantized State Lasing of a Current Pumped Single Quantum Well Laser", Appl. Phys. Lett., Vol. 49, No. 25, pp. 1689-1691, 1986.

8. H. Okamoto, "Semiconductor Quantum-Well Structures for Optoelectronics - Recent Advances and Future Prospects", Jpn., J. Appl. Phys., Vol. 26, No. 3, pp. 315-330, 1987.

9. A. Larsson, M. Mittelstein, Y. Arakawa, and A. Yariv, "High-Efficiency Broad-Area Single-Quantum-Well Lasers with Narrow Single-Lobed Far-Field Patterns Prepared by Molecular Beam Epitaxy", Electron. Lett., Vol. 22, No. 2, pp. 79-81, 1986.

10. A. Larsson, J. Salzman, M. Mittelstein, and A. Yariv, "Lateral Coherence Properties of Broad-Area Semiconductor Quantum Well Lasers", J. Appl. Phys., Vol. 60, No. 1, pp. 66-68, 1986.

11. C. P. Harder, P. Buchmann, and H. Meier, "High-Power Ridge-Wave-Guide AlGaAs GRIN-SCH Laser Diode", Electron. Lett., Vol. 22, pp. 1081-1082, 1986.

12. D. F. Welch, M. Sakamoto, G. H. Harnagel, W. Streifer, D. R. Scifres, J. G. Endriz, "High Power Single Mode Semiconductor Laser", SPIE Meeting OE Lase Proceedings, Vol. 1043, Paper 08, Los Angeles CA, Jan. 1989.

13. P. L. Derry, A. Yariv, K. Y. Lau, N. Bar-Chaim, K. Lee, and J. Rosenberg, "Ultralow-Threshold Graded-Index Separate-Confinement Single Quantum Well Buried Heterostructure (Al,Ga)As Lasers with High Reflectivity Coatings", Appl. Phys. Lett., Vol. 50, No. 25, pp. 1773-1775, 1987.

14. P. L. Derry, T. R. Chen, Y. Zhuang, J. Paslaski, M. Mittelstein, K. Vahala, A. Yariv, K. Y. Lau, and N. Bar-Chaim, "Properties of Ultra Low Threshold Single Quantum Well (Al,Ga)As Lasers for Computer Interconnects", Optoelectronics - Devices and Technology, Vol. 3, No. 2, pp. 117-130, 1988.

15. S. H. Macombes, J. S. Mott, R. J. Noll, G. M. Gallatin, E. J. Gratrix, and S. L. O'Dwyer, "Surface-Emitting Distributed Feedback Semiconductor Laser", Appl. Phys. Lett., Vol. 51, No. 7, pp. 472-474, 1987.

16. K. Mitsunaga, M. Kameya, K. Kojima, S. Noda, K. Kyuma, K. Hamanaka, and T. Nakayama, "CW Surface-Emitting Grating-Coupled GaAs/AlGaAs Distributed Feedback Laser with Very Narrow Beam Divergence", Appl. Phys. Lett., Vol. 50, No. 25, pp. 1788-1790, 1987.

17. D. F. Welch, R. Parke, A. Hardy, W. Streifer, and D. R. Seifres, "High-Power Grating-Coupled Surface Emitters", Electron. Lett., Vol. 25, No. 13, pp. 819-820, 1989.

18. F. Koyama, S. Kinoshita, and K. Iga, "Room-Temperature Continuous Wave Lasing Characteristics of a GaAs Vertical Cavity Surface-Emitting Laser", Appl. Phys. Lett., Vol. 55, No. 3, pp. 221-222, 1989.

19. J. L. Jewell, K. F. Huang, K. Tai, Y. H. Lee, R. J. Fisches, S. L. McCall, and A. Y. Cho, "Vertical Cavity Single Quantum Well Laser", Appl. Phys. Lett., Vol 55, No. 5, pp. 424-426, 1989.

20. H. Z. Chen, A. Ghaffari, H. Morkoc and A. Yariv, "Effect of Substrate Tilting on Molecular Beam Epitaxial Grown AlGaAs/GaAs Lasers Having Very Low Threshold Current Densities", Appl. Phys. Lett., Vol. 51, No. 25, pp. 2094-2096, 1987.

21. E. Yablonovitch, and E. O. Kane, "Reduction of Lasing Threshold Current Density by Lowering of Valence Band Effective Mass", IEEE J. Lightwave Tech., Vol. LT-4, No. 5, pp. 504-506, 1986.

22. E. Kapon, J. P. Harbison, C. P. Yun, and N. G. Stoffel, "Patterned Quantum Well Semiconductor Injection Laser Grown by Molecular Beam Epitaxy", Appl. Phys. Lett., Vol. 52, No. 8, pp. 607-609, 1988.

23. N. Hamao, M. Sugimoto, N. Takado, Y. Tashiro, H. Iwata, T. Yuasa, and K. Asakawa, "Surface-Emitting GaAs/AlGaAs Lasers with Dry-Etched 45° Total Reflection Mirrors", Appl. Phys. Lett., Vol. 54, No. 24, pp. 2389-2391, 1989.

24. H. Zarem, K. J. Vahala, and A. Yariv, "Gain Spectra of Quantum Wires with Inhomogeneous Brodening", IEEE J. Quantum Elect., Vol. QE-25, No. 4, pp. 705-712, 1989.

25. K. J. Vahala, "Quantum Box Fabrication Tolerance and Size Limits in Semiconductors and Their Effect on Optical Gain", IEEE J. Quantum Elect., Vol. QE-24, No. 3, pp. 523-530, 1988.

26. A. Yariv, and M. Mittelstein, "Quantum Confined Lasers", Optical Fibers Communication Conference, Paper Tu H1, Houston, Texas, Feb. 1989.

2.11 Appendix

The evaluation of the alternate laser structures for optical interconnects presented in the talk prepared in the summer of 1989 have to be updated by the very encouraging results on **vertical cavity strained quantum well lasers** presented first at the OPTICS '89 Conference in Orlando, Florida by several groups mainly from AT&T Bell Labs. The hindrance for low threshold current of vertical cavity lasers had been the high required gain-coefficient to provide for non-reflected light in the very short cavity. The key to make low threshold currents which are now as low as the best etch emitting lasers (<1 mA) is **very high reflectivity of the mirrors.** In excess of **0.995** reflectivity results in a reduction of the required gain such that even a single quantum well can provide the gain of a vertical cavity semiconductor laser.

The new accomplishment have been achieved with **multiple period dielectric mirrors formed by GaAlAs and AlAs layers** epitaxially grown below and above the active region. Since then further development provided lasers with are passivated, buried in polyimide or defined by ion implantation such that the initial direct exposure of the lasers has been eliminated.

3 DESIGN OF LASER STRUCTURES

The laser structure and variations as used in this research and development effort are described and put in perspective to alternatively used laser structures.

3.0 Abstract

The selection of the ring structure as the candidate for the laser is described. The two lateral structures - buried heterostructure and ridge wave-guide - are introduced and the second order Bragg reflector as a vertical output coupler is explained. Considerations about the placement of the grating in lasers are added.

3.1 Structures for Vertical Emitting Ring Lasers

As mentioned in chapter one the main part of this contract work is our ring resonators research and development effort. This provides a selection of options for the detailed structure to be investigated.

The structure we envisioned for the light source of an optical interconnect is a GaAs/GaAlAs semiconductor laser utilizing a **curved real index wave-guide forming a ring structure for the resonator and a second order distributed Bragg reflector grating for vertical output coupling** as illustrated in **Figure 31**. This ring resonator is the only structure that does not rely on facets, therefore it is free

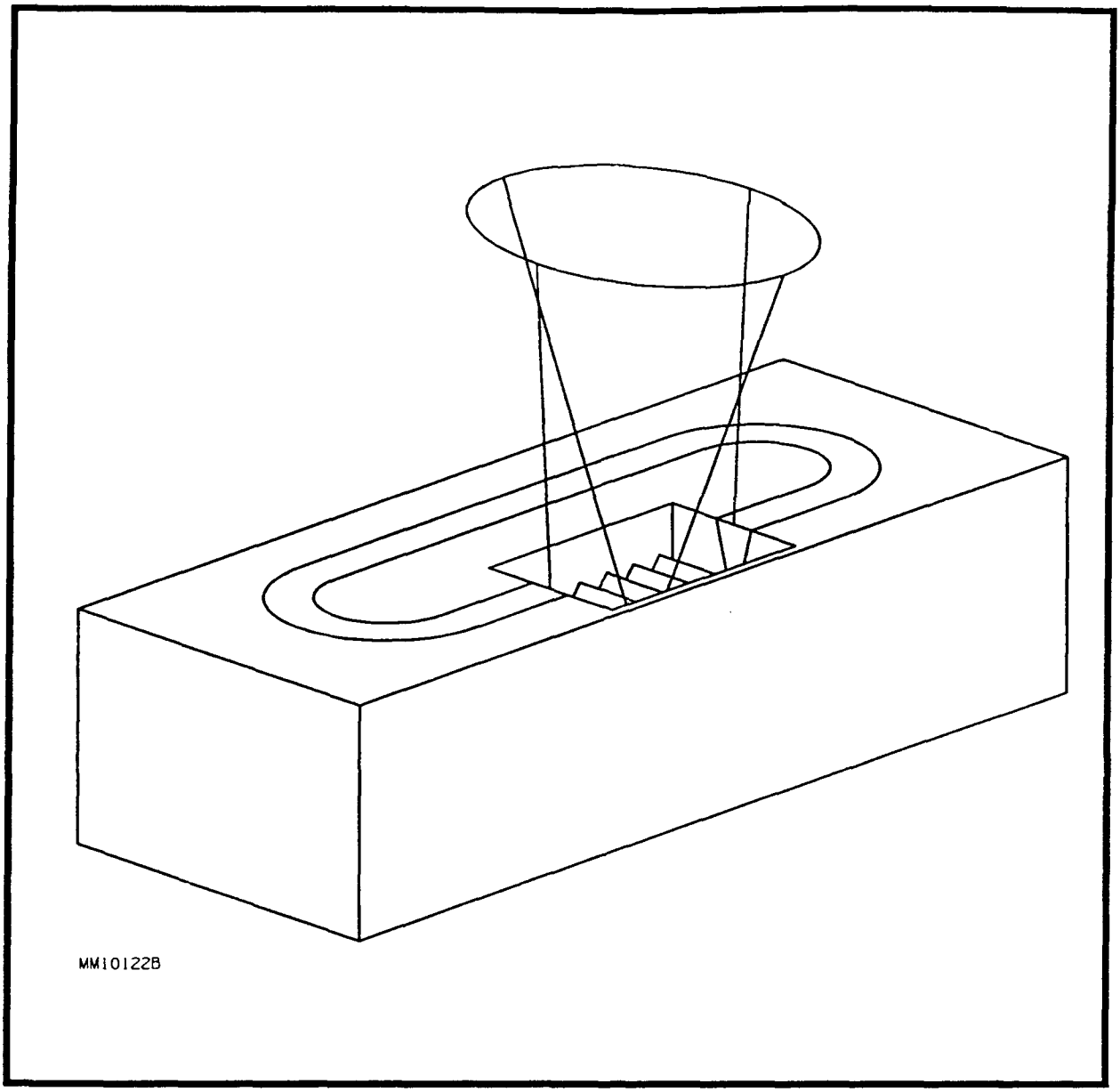

Fig. 31 Perspective drawing of proposed ring laser structure. The elongated ring in the middle of the semiconductor chip is shown with a trench etched down to a surface grating from which the output beam emerges vertically.

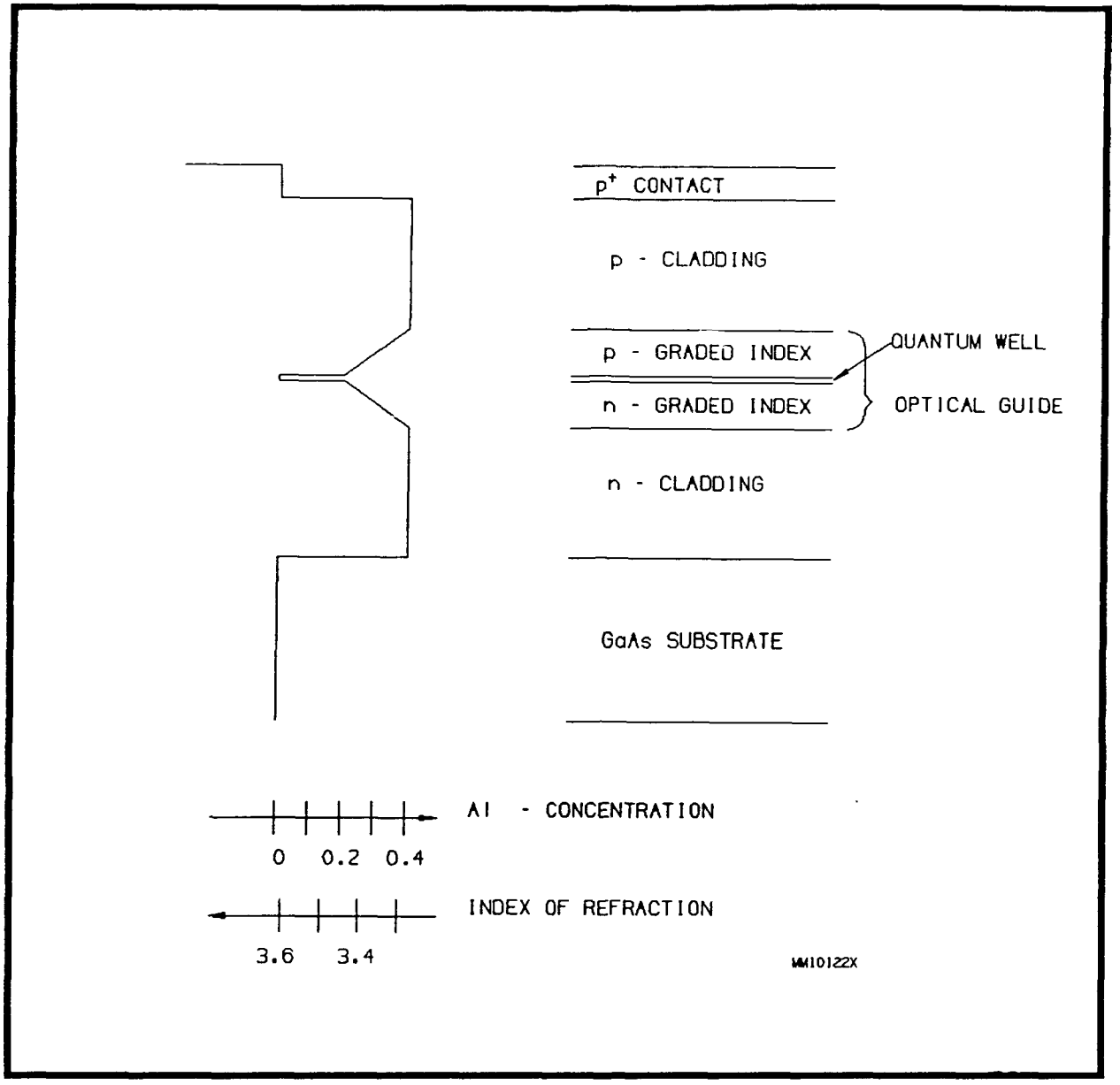

Fig. 32 Schema of layer-structure used for buried single quantum well lasers. The Aluminium concentration as a function of position in the grown material is shown vertically and the approximate index of refraction at the lasing wavelength is indicated.

from constraints on the edge of the chip and does not require optical quality non-planar etched facets. The intention is to minimize critical processing steps which reduce the reproducibility of the device fabrication in order to develop a process that has high yield - a pre-requisite for multiple laser monolithic integration.

For the **transverse** wave-guide in the GaAs/GaAlAs material (that is the layer structure) a **graded index separate confinement heterostructure** is utilized. The active region in the center of the guiding structure is a single quantum well (**Figure 32**) in most cases, in same cases more quantum wells as added to form a multiple quantum well structure.

For the **lateral** wave-guide two structures have been investigated. This wave-guide has to be real index guiding in order to reduce the bending losses so that compact rings can be fabricated. First a **buried structure** based on a single quantum well material was examined. Even so, encouraging good results have been obtained, the reproducibility of very low threshold curved lasers has not been established. Second a **ridge wave-guide structure** based on single and also multiple quantum well material was fabricated. Development of this structure has not been carried through to minimize threshold currents, however, lasing of half ring structures has been achieved.

The integration of the **vertical output grating coupler** depends on the lateral structure utilized. In all cases the grating has to be placed within the region of the transverse optical wave-guide where the electromagnetic field is high such that the corrugation in the structure provides a sufficient change in effective index for refraction. In particular gratings on the semiconductor surface have been investigated.

3.2 Buried Heterostructure Single Quantum Well Structure

To develop a ring resonator in the plane of the substrate with vertical output coupling several structures can be considered for implementation. Targeting a low threshold design, the first structure investigated is a buried heterostructure lateral wave-guide with a single quantum well active region. This structure has been extensively researched at ORTEL Corporation and ultra low thresholds of 0.55 mA for coated straight lasers have been obtained previously. As explained in section 2.2 low threshold current densities can be maintained for single quantum well structures as long as the required modal gain is moderate (not exceeding 30 cm^{-1}). If the losses of the ring resonator design can be held within this gain requirement for a small enough devise **low threshold currents** should be obtainable.

Theoretically a **narrow active region with strong lateral index step** is desirable in order to reduce the size of the optical

mode and more importantly reduce the bending losses for a given radius of curvature. Experimentally, narrow active regions are very demanding to fabricate due to the small tolerances that have to be met and the orientation dependent etching encountered in wet etching preformed after photolithographic patterning. Indeed low threshold currents were obtained in half ring laser test structures as described in section 6.1. However, the complex processing required has lead us to consider alternative structures. The fabrication process for the ring lasers has not included the grating fabrication for vertical output coupling at that stage of the development. This added complexity requires a reproducible process for the ring wave-guide fabrication in order to achieve yields beyond those achieved in feasibility demonstration.

3.3 Ridge Wave-guide Quantum Well Structure

In order to develop a structure less demanding in processing requirements ridge wave-guide structures have been investigated. The ridge wave-guide structure relies on removal of cladding layer material on the upper side of the active region only. Consequently the active region is not touched during the processing and thereby no defects are introduced as compared to the buried structure. More importantly **no regrowth is involved in creating the lateral real index wave-guide.** This is the kind of processing simplification we were seeking in trying an alternative lateral guiding structure. While the

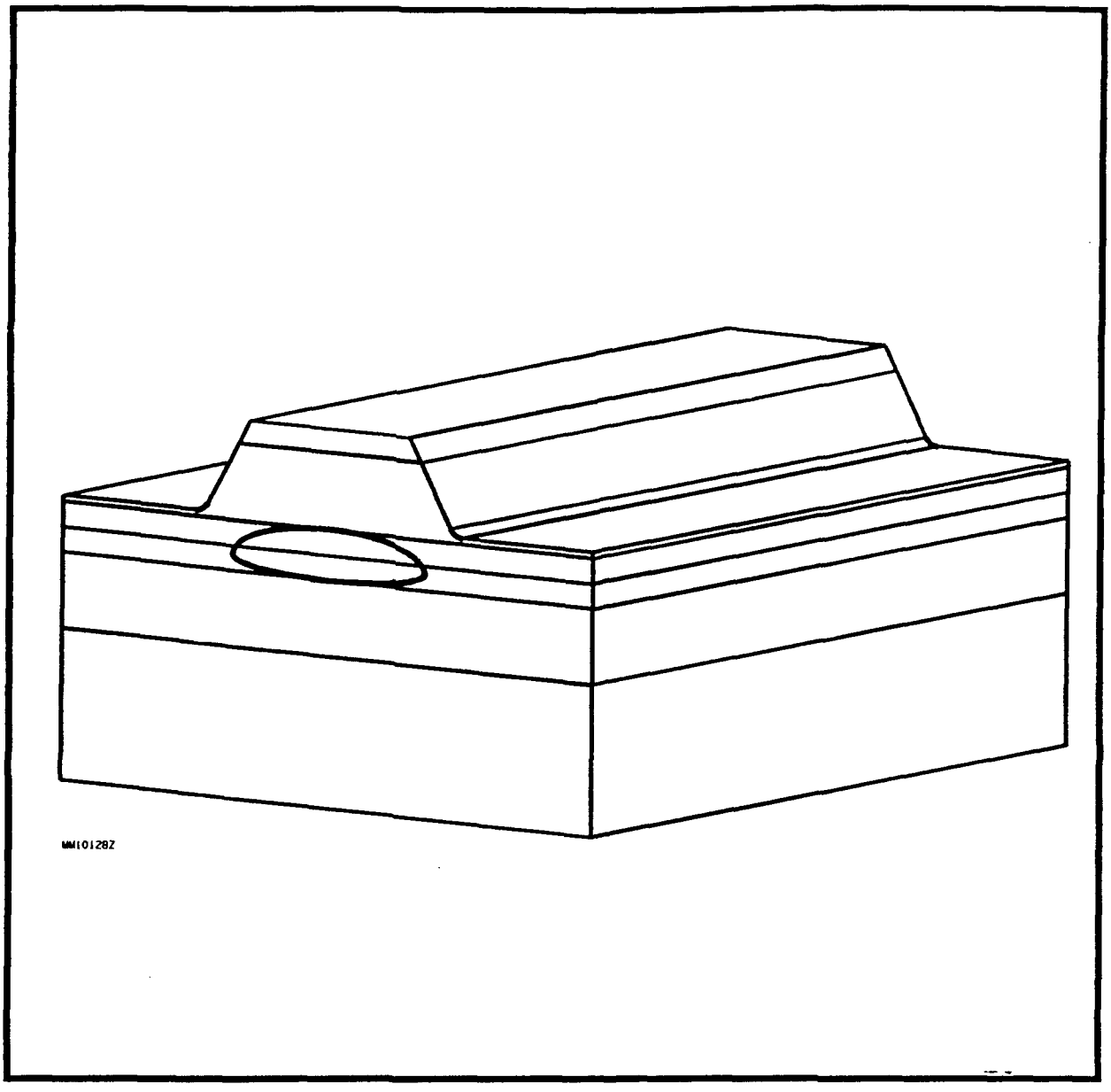

Fig. 33 Ridge wave-guide structure. The cross-section is evident to the lower left hand side while the non-planar surface is shown to the upper right.

buried structure fabrication includes a more or less successful planarization accomplished by the regrowth, the ridge wave-guide structure fabrication leaves inherently a non-planar top surface of the wafer. **Figure 33** shows the schematic of the ridge wave-guide structure.

Experimentally the non-planar top surface is significant for subsequent processing. A more important consequence is an increased width of the active region and a reduced strength of the lateral guiding of the ridge wave-guide as compared to the buried heterostructure. Consequently the design exhibits an increased area of the active region and increased bending losses. Theoretically the **bending losses can be reduced by an asymmetric design** of the lateral wave-guide in which at the outside of the bend a deeper removal of cladding material is performed. We did not get to try this idea within this research and development effort. Test lasers with a single quantum well active region did not overcome the losses, however, a **multiple quantum well active region provided sufficient gain to obtain lasing** of half ring laser test structures as described in section 7.6.7. The ridge wave-guide structure leads itself to integration of surface gating for vertical output coupling as described in section 8.3 .

3.4 **Second Order Bragg Reflector**

Gratings are used for **wavelength selective beam directing** in many applications. In most cases a **extended beam** of electromagnetic radiation impinges on a large number of periods of the grating in **parallel.** This configuration is chosen, because the pointing precision of the redirected beam is determined by the precision of the definition of the direction of the incoming beam in the non-guided case. A larger beam diameter fundamentally gives a possible better definition of the beam direction.

However, in the case of the vertical output coupler of a semiconductor as considered in this research and development effort, the **incoming electromagnetic radiation is guided.** In fact, the input to the grating is tightly confined in a single transverse mode and **the grating is in the plane of propagation.** Consequently the radiation strikes on the periods of the grating in **serial.** Each period constitutes only a small perturbation in the wave-guide such that the majority of the input is simply transmitted and only a small fraction is refracted or scattered. In this way **hundreds or even thousands of periods of the grating contribute to the output.**

In particular the intention is to use a **second order Bragg reflector configuration.** That means, an addition of two

wavelength per grating period provides an in-phase retro-reflection back into the wave-guide propagating in the opposite direction as compared to the input beam. Considering the case of one additional wavelength per grating period it is found that the output beam emerges **perpendicular to the grating** and therefore perpendicular to the wave-guide. This **grating coupled first order beam constitutes the vertical output** from the ring laser design.

In an open resonator - utilizing a single ended second order Bragg reflector - the second order is used to provide **feedback** to the active region and therefore the lasing wavelength is grating period defined. However, in the case of the ring resonator feedback is not required because the resonator is closed and the transmitted light (0-th order) is fine for the closure of the resonator condition. Consequently **the lasing wavelength is not necessarily grating period defined.** Furthermore, **it is questionable if the grating period defined wavelength is the desired operational point of the second order grating ring laser.** The counter-propagating beam in the ring are coupled by the grating and contribute constructively to the output beam, thereby increasing the output coupling and consequently **increasing** the gain **requirement** of the resonator. However in steady state lasing occurs at the lowest possible pump strength that the resonator configuration provides.

If narrow spectral band or single frequency lasing occurs in a ring laser with second order grating, then the output beam is expected to be as narrow as the contributing part of the grating is long. The coherent emission of a one dimensional aperture of length l at a wavelength λ provides for constant amplitude flat phase front in the near field a far field pattern of angular full width at half maximum intensity α where $\alpha = 50.76° * \lambda / l$. For example for a **grating length of only 40 µm** the **far field angle** full width at half intensity maximum in the direction of the grating is expected to be already **near 1° wide.**

3.5 Implementing the Grating Output Coupler

Second order gratings for vertical emission perpendicular to a single mode wave-guide have to be positioned such that the local intensity of the optical field at the position of the grating is high enough for good efficiency with moderate grating depth. Consequently the grating has to be within the wave-guiding structure. Basically two options exist:

A) Grating within semiconductor material. A grating etched into the substrate and then buried under a single growth layer structure in the GaAs/GaAlAs system is not compatible with forming a wave-guide unless the substrate already has an epitaxial GaAlAs layer. In order to define the grating with conventual methods within the semiconductor material requires

a **two step growth process.** The grating is lithographically defined after completion of the first growth, etched and preserved to be buried under the material deposited in the second growth. This second growth is not useful for lateral optical guiding and electrical blocking layers often provided by the second growth, an additional third growth would be required to implement these additional properties.

B) Grating on semiconductor surface. A grating etched into the uppermost layer of semiconductor material can be utilized providing that this layer is part of the optical wave-guiding structure such that high optical intensity is achieved. The relative low index of refraction outside the semiconductor material provides a **strong guiding effect with tends to expel the optical field** from the guided mode. However by locating the layer with the grating near the center of the original wave-guide and etching the topside layers away adequate optical field intensity can be provided. This leads to a strong modification of the optical mode, but the single mode guiding characteristics can be maintained. Typically the transverse optical mode size inside a GaAs/GaAlAs lasers is in the range of 0.2 to 0.5 μm full width at half maximum intensity. In single quantum well lasers the well is almost always placed in the center of the optical mode. Consequently the **layer of the grating has to be placed very close to the well with about 0.1 μm accuracy.**

4 ACHIEVING BURIED RING STRUCTURES

The experiments performed to step up to the proposed laser structure are described.

4.0 Abstract

The qualification of wafer material for the proposed laser is described. Subsequently the low threshold operation of buried heterostructure quantum well lasers with a straight resonator is confirmed. For the ring structure a simplified processing that excludes the very low threshold potential is utilized in the first proof of concept lasers.

4.1 Material Test Lasers

Previously at ORTEL Corporation single quantum well material has been grown and characterized in order to fabricate ultra low-threshold lasers. The basic structure is a graded-index separate-confinement heterostructure (**GRINSCH**) single quantum well. The growth took place in our low-pressure metal-organic chemical vapor phase deposition (**MOCVD**) reactor. The sources used were: Trimethyl Gallium, Trimethyl Aluminum, Diethyl Zinc and Hydrogen Selenide. The growth has been performed at a temperature of 750°C at a pressure of 80 torr with an average gas flow of 15 liters/minute.

The following layers were grown on n^+ GaAs substrate: 0.5 μm n^+ - GaAs buffer layer, 1.5 μm n - $Al_{0.4}Ga_{0.6}As$ cladding layer, 0.2 μm graded n - $Al_xGa_{1-x}As$ layer (x = 0.4 to 0.2), 150 Å undoped GaAs quantum well, 0.2 μm undoped $Al_xGa_{1-x}As$ layer (x = 0.2 to 0.4) and 1.5 μm p - $Al_{0.4}Ga_{0.6}As$ cladding layer.

At first, **broad stripe lasers** (~100 μm wide, 500 μm long) were fabricated from the grown material. Typical threshold current densities range from 250 A cm^{-2} to 500 A cm^{-2}. An important step in **material qualification** was to **anneal** the material at elevated temperatures in the range of 700-800°C for 2 hours in order to **simulate** the temperature cycle required for **regrowth**, which is the next step in fabricating buried-heterostructure lasers. It was found that the best results, i.e. threshold current densities change negligibly, were obtained for annealing temperatures in the range of 700-750°C. Material was also characterized by measuring room temperature photo-luminescence as well as carrier concentrations and mobilities.

4.2 Buried Quantum Well Test Lasers

Utilizing material with a moderately thick single quantum well of 150 Å straight test lasers were fabricated as follows: 1.5 μm wide mesas along the (0 $\bar{1}$ 1) crystal orientation were produced by etching through the MOCVD grown layers into the substrate. A 0.5 μm p-$Al_{0.5}Ga_{0.5}As$ followed by a 3.0 μm n-$Al_{0.5}Ga_{0.5}As$ layer were grown by liquid phase epitaxy (**LPE**) to provide

electrical and optical lateral confinement. A shallow Zn diffusion was performed to facilitate the ohmic contact on the p-side metal contact (chromium-gold) of the device metallization: The wafer was then lapped, backside metallized (gold-germanium, nickel, gold) and the contacts were alloyed.

Best lasers, with a cavity length of 250 μm, had a threshold current of 4 mA (with uncoated mirrors) and slope efficiency of 0.4 W A^{-1} to 0.5 W A^{-1} (from one mirror). After coating the back side with high reflectivity (~0.7) dielectric coating (quarter-wave aluminum oxide followed by quarter-wave silicon) the threshold current decreased to ~3 mA and the slope efficiency (from the front mirror) increased to ~0.75 W A^{-1}. An additional similar high-reflectivity coating on the front mirror resulted in further reduction of the threshold current to ~2 mA while restoring the slope efficiency to the original value of 0.4 W A^{-1} to 0.5 W A^{-1}.

These results verify our original considerations that unlike conventional double-heterostructure lasers, enhancement of the facet reflectivity of quantum well structures lead to a substantial reduction of the threshold current, without paying any significant penalty in the quantum efficiency of the devices. This is basically due to the lower current density needed to make the transverse structure with the thin active layer transparent and the low distributed losses in the crystal.

4.3 Buried Heterostructure Ring Test Lasers

Next ring double-heterostructure lasers with both first and second growth performed by LPE were fabricated. In this case the **active region is approximately 1000 Å thick.** The fabrication is simpler and the thick active region will provide ample gain to the optical mode, however, very low threshold currents cannot be obtained from this structure. This study was performed as a preliminary step to fabricate such lasers using MOCVD quantum well material. The basic process is similar to the one outlined above, with the main difference (in addition to having a double heterostructure) being the use of a curved lateral wave-guide structure. The devices fabricated consisting of **half a ring** with a diameter of 150 μm. The advantage of such a structure is that both mirrors are cleaved at the same crystal facet, eliminating the necessity for two cleavages. As explained in chapter one, this leaves room on the wafer for fabricating electronic components without being limited to small areas. These lasers typical have threshold currents of 40 mA and slope efficiency of 0.2 W A^{-1} to 0.3 W A^{-1} (both facets). Straight reference lasers from the same wafer displayed threshold currents of 10 mA to 20 mA and slope efficiencies of 0.6 W A^{-1} to 0.8 W A^{-1} (adding both facets). The difference in performance is due to the bending loss of the curved wave-guide.

5 BURIED RING QUANTUM WELL STRUCTURE

A half-ring structure is described[0] since it allows all the testing of the curved wave-guide without the added complexity of the output coupler. The full ring lasers and their intention for optical interconnect is not included here but rather described in the following chapter.

5.0 Abstract

Half-ring geometry single quantum-well GaAlAs have been fabricated. These lasers rely on a single cleave to obtain both resonator end-reflectors. Using a buried heterostructure wave-guide for lateral confinement and a high reflectivity facet coating, threshold currents as low as 14.5 mA and a frequency response extending to 6.5 GHz have been achieved.

5.1 Introduction

The vast majority of semiconductor lasers rely on a Fabry-Perot cavity formed by two cleaved facets. The fabrication simplicity of this optical resonator is very desirable. However, when the laser is to be integrated monolithically with other electronic and/or electro-optical components, the need for cleaved facets

constitutes a severe constraint, so that alternative resonator configurations are desired. Micro-cleaving, a local shallow cleave, can be employed, but requires difficult processing.[1]

Etched facets and/or folding mirrors for the optical path have been used but these designs have not yet come close to the reported very low threshold currents achieved with double cleaved coated resonator buried heterostructure lasers.[2,3] In the case of narrow stripe real index wave-guide lasers, however, the **need for a second facet can be eliminated by introducing a 180° turn in the optical wave-guide and placing both ends of the laser cavity at the same cleave.**[4] Minimizing the bending loses should make possible very low threshold currents comparable to those of conventional double cleaved Fabry-Perot cavity lasers.

Lasers with curved wave-guide active regions have been previously reported.[4-9] In this letter we report on a low threshold current density structure and high frequency response measurements on half-ring lasers fabricated using a narrow lateral buried heterostructure and a **single quantum-well graded index separate confinement transverse structure.**

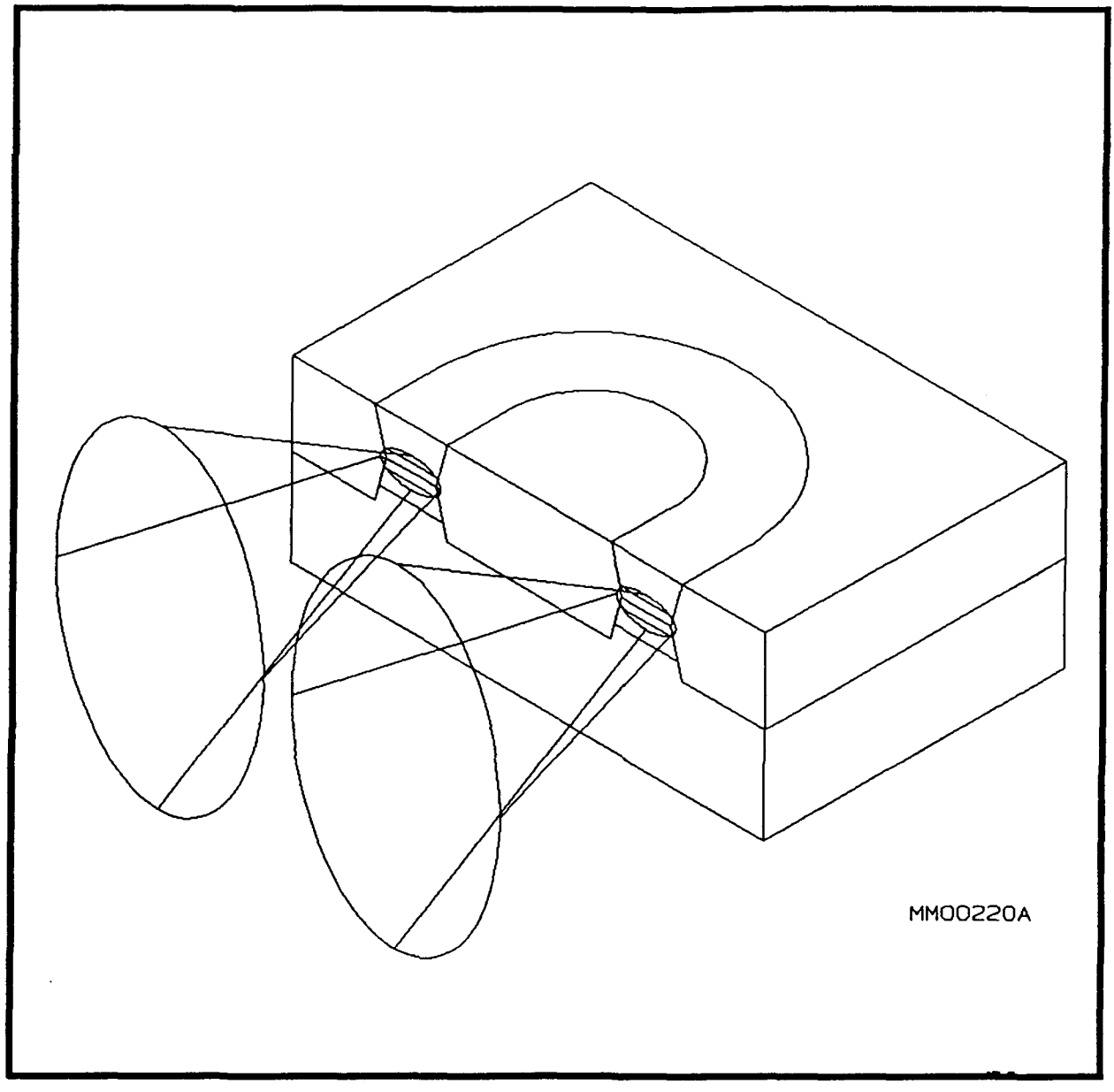

Fig. 51 Schematic view of the 180° curved wave-guide buried heterostructure single quantum-well graded index separate confinement heterostructure laser which utilizes a single facet. The two output beams emerge to the lower left, the facet shows the buried structure and the top shows the half-ring shape of the wave-guide.

5.2 Experimental Approach

To demonstrate the feasibility of single facet curved wave-guide buried heterostructure lasers, devices were fabricated using a two step epitaxial growth technique. In the first growth a single quantum-well graded index separate confinement heterostructure (**SQW GRINSCH**) in GaAs/GaAlAs was grown by metal-organic-chemical vapor phase deposition (**MOCVD**). This structure provides the vertical mode guide and is known for its low distributed wave-guide losses as well as very low current densities required to reach modal gains of approximately 30 cm^{-1} [10-12]

After photolithographic patterning, most of the surface area was etched down to the substrate, leaving mesas with a smooth 180° turn extending on both sides into straight sections. The stripe width of about 1.5 µm at the position of the quantum-well defines the active region of the laser. In the second growth, electrical blocking and lateral optical guiding layers of GaAlAs were grown by liquid phase epitaxy (**LPE**). **Cleaving once through both straight sections near the transition from the curved part provides two reflectors for the optical cavity.** This gives these lasers a half-ring appearance. A schematic view of the structure with its single cleaved facet is shown in **Figure 51** .

5.3 Experimental Findings

Half-ring lasers were fabricated with **different radii to investigate losses due to wave-guide curvature.** Of those studied, a 100 μm radius device led to the lowest threshold current of 14.5 mA for half-ring lasers with a high reflectivity coating (nominal R=0.90). For a radius of 150 μm a 20.5 mA threshold current was obtained for a similar structure. While **the coating lowered the threshold** by at least 60% for the smaller radius devices, the reduction was only 35% for the larger devices. This is probably due to the relatively **high gain required to sustain lasing in the uncoated 100 μm radius half-ring laser** (estimated to exceed 70 cm^{-1}) with respect to the modal gain a single quantum-well structure can provide with low current densities[11,12]. Reducing the radius to 50 μm made lasing impossible. Using data from similar straight lasers the losses due to curvature at 50 μm are estimated to be beyond 100 cm^{-1} in the present devices.

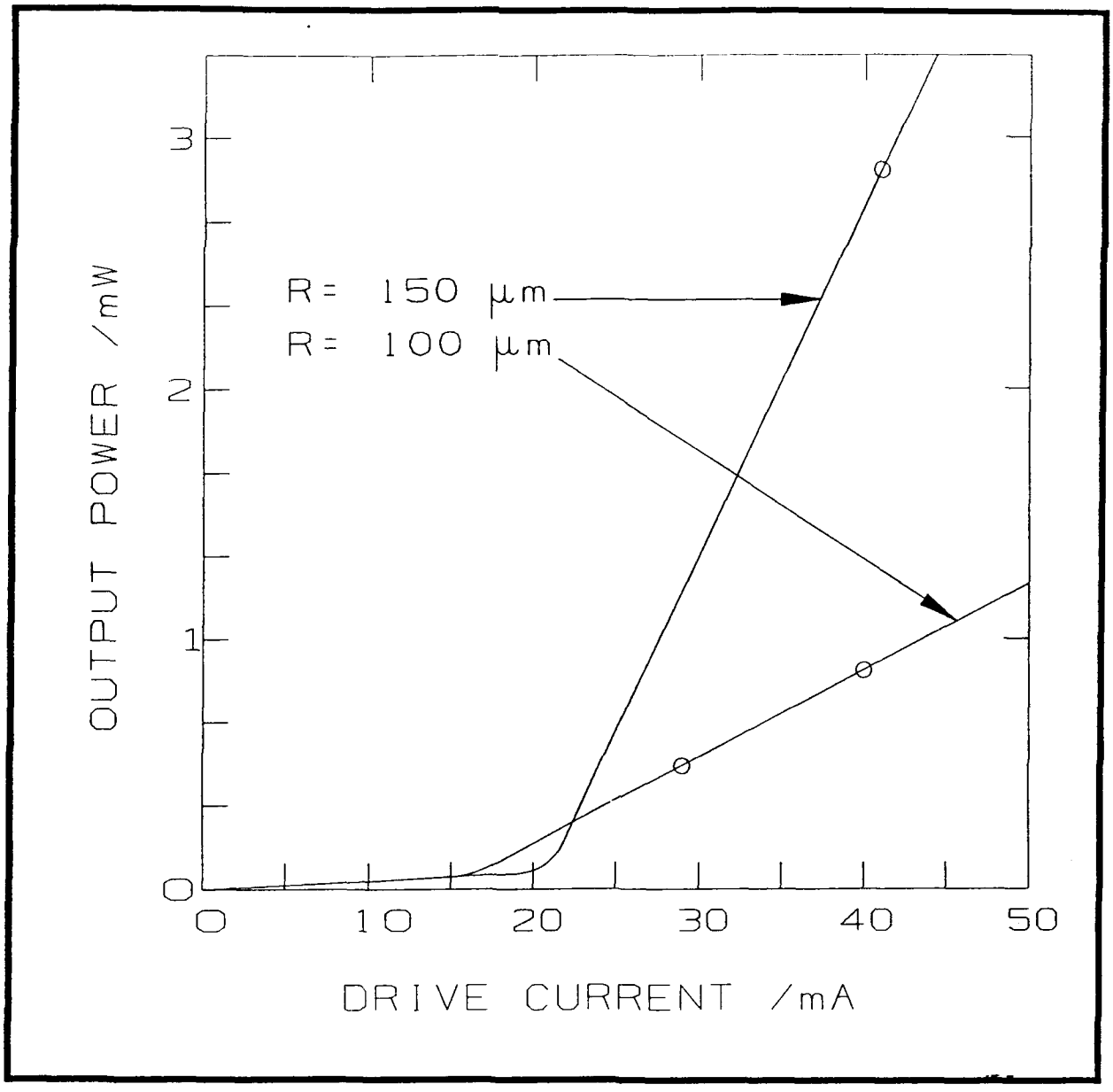

Fig. 52 The light output versus pump current input characteristic of the coated half-ring lasers operated cw with radii of curvature of 150 μm and 100 μm. The marks at 41 mA, 29 mA, and 40 mA respectively indicate the bias points for the high frequency response measurements.

5.4 Evaluating Slope Efficiency

Additional information can be obtained from measurements of the slope efficiency. The slope efficiency is proportional to the ratio of the **losses associated with output coupling** to the total losses. The **total losses** are comprised of output coupling losses, distributed losses like scattering and absorption in the wave-guide, and losses due to curvature. The measured values of the slope efficiency for the 150 μm half-ring lasers with high reflection coatings is 4 times larger than for the corresponding 100 μm half-rings. The absolute slope efficiencies of the present half-ring quantum-well lasers are, 0.14 W A^{-1} and 0.035 W A^{-1} for the 150 μm and 100 μm radius devices, respectively. The large ratio seems to indicate the substantial increase in losses due to curvature when the radius is reduced from 150 μm to 100 μm . The light output versus pump current characteristic of the cw operated coated half-ring lasers with radius of curvature of 150 μm and 100 μm are presented in **Figure 52**. Note that the output at high currents is actually decreased by the coating due to the resulting low quantum efficiency.

5.5 High Speed Modulation Results

To demonstrate the high speed potential of single quantum-well ring lasers, the microwave modulation response of half-ring

lasers with high reflectivity coatings was measured. Lasers with radius of curvature of 150 μm and 100 μm were operated at two times the threshold current with a **superimposed high frequency modulation current**, and achieved a -3 dB bandwidth of nearly 5 GHz. The smaller device with a threshold current of 14.5 mA achieved a **-3 dB bandwidth of 6.5 GHz when biased at 40 mA**. These half-ring devices are thus as fast as their straight counterparts that were fabricated for comparison.

5.6 Summary

In summary, half-ring laser structures utilizing buried heterostructure lateral waveguides and single quantum-well separate confinement graded index transverse structures have been fabricated. Preliminary experimental results include half-ring device lasing threshold currents as low as 14.5 mA and frequency response as high as 6.5 GHz.

5.7 References

0 Nadav Bar-Chaim, Kam Y. Lau, M.A. Mazed, Michael Mittelstein, Se Oh, Jeffrey E. Ungar, and Israel Ury, "Half-Ring Geometry Quantum-Well GaAlAs Lasers", Appl. Phys. Lett., **57** (10), 966-967 (1990).

1 H. Blauvelt, N. Bar-Chaim, D. Fekete, S. Margalit, and A. Yariv, "AlGaAs Lasers with Micro-Cleaved Mirrors Suitable for Monolitic Integration"; Appl. Phys. Lett., **40**, 289 (1982).

2 K. Y. Lau, P.L. Derry, and A. Yariv, "Ultimate Limit in Low Threshold Quantum Well GaAlAs Semiconductor Lasers", Appl. Phys. Lett., **52**, 88 (1988).

3 P. L. Derry, A. Yariv, K. Y. Lau, N. Bar-Chaim, K. Lee, and J. Rosenberg, "Ultralow-Threshold Graded-Index Separate-Confinement Single Quantum Well Buried Heterostructure (Al,Ga)As Lasers with High Reflectivity Coatings", Appl. Phys. Lett., **50**, 1773 (1987).

4 N. Matsumoto, H. Kawaguchi, and K. Kumabe, "Oscillation Characteristics of Semiconductor Lasers with Circular Waveguides", JPN. J. Appl. Phys., **16**, 1885-6 (1977), and International Conference on Integrated Optics and Optical Fiber Communications, Tokyo and Osaka 189 (1977).

5 I. Ury, S. Margalit, N. Bar-Chaim, M.Yust, D. Wilt, and A. Yariv, "Whispering Gallery Lasers on Semi-Insulating GaAs Substrates", Appl. Phys. Lett. **36**, 629 (1980).

6 A. S.-H. Liao and S. Wang, "Semiconductor Injection Lasers with a Circular Resonator", Appl. Phys. Lett. **36**, 801 (1980).

7 H. Ismail, A. Fattah, and S. Wang, "Semiconductor Interferometric Laser", Appl. Phys. Lett., **41**, 112 (1982).

8 S. Wang, H.K. Choi, and I.H.A. Fattah, "Studies of Semiconductor Lasers of the Interferometric and Ring Types", IEEE J. Quantum Electron **QE-18**, 610 (1982).

9 A.F. Jezierski and P.J.R. Laybourn, "Integrated Semiconductor Ring Lasers", IEE Proceedings **135**, 17 (1988).

10 M. Mittelstein, Y. Arakawa, A. Larsson, and A. Yariv, "Second Quantized State Lasing of a Current Pumped Single Quantum Well Laser", Appl. Phys. Lett., **49**, 1689 (1986).

11 Michael Mittelstein, "Theory and Experiments on Unstable-Resonator and Quantum-Well GaAs/GaAlAs Lasers", Ph.D. Thesis, California Institute of Technology, Pasadena, CA, (March 1989).

12 M. Mittelstein, I. Ury, N. Bar-Chaim, K. Y. Lau, and J. Ungar, "Ultralow Threshold Quantum Well Lasers For Computer Interconnects", , SPIE OE/Fiber '89, Symposium on optical interconnects in the computer environment, Boston Massachusetts, Sep. 7. 1989, and SPIE Proceedings, **1178**, 177-187 (1989).

6 BURIED LASERS: CHAMPION RESULTS AND REPRODUCIBILITY

Best obtained results not presented in the previous chapter are described. However, fabrication of consistent high quality devices could not be achieved. Results as described in the previous chapter were hard to reproduce. A detailed description of properties of single quantum well lasers with regard to device degradation due to imperfections is presented in order to provide background for the decision to try alternate structures to the buried designs. A comparison to and introduction of the ridge wave-guide structure is given.

6.0 Abstract

Single quantum well buried structure ring lasers have been fabricated and obtained high performance of devices are presented. The specific required gain dependent device degradation of single quantum well material is discussed. A comparison buried versus ridge wave-guide structure is given.

6.1 Champion Buried Quantum Well Ring Lasers

The layer structure utilizes a single quantum well in a graded-index separate-confinement heterostructure (SQW GRINSCH). The growth was performed in our low-pressure metal-organic chemical-vapor deposition (MOCVD) reactor. Grown on a n^+ GaAs substrate are the following layers: an n-cladding

layer of $Ga_{0.6}Al_{0.4}As$, an n-doped layer graded to $Ga_{0.8}Al_{0.2}As$, a 100 Å undoped GaAs quantum well, a p-doped layer graded from $Ga_{0.8}Al_{0.2}As$ to $Ga_{0.6}Al_{0.4}As$, and a p-cladding layer of $Ga_{0.6}Al_{0.4}As$.

The structure was etched down into the substrate to define rings and stripes of a width of 1 to 1.5 µm at the quantum well layer. A liquid phase epitaxy (LPE) regrowth of p- and n-doped blocking layers of $Ga_{0.6}Al_{0.4}As$ was performed serving as lateral index guide for the active structure. After appropriate metallization, devices were cleaved. Half-ring lasers using only one crystal facet for both mirrors were obtained.

The threshold current and slope efficiency of half ring and straight reference lasers were determined under as cleaved and coated continuous wave (CW) operation conditions. The coatings used increased the reflectivity from 0.3 to about 0.7 and 0.9 respectively resulting in reduced output coupling and reduced threshold currents.

While the straight reference lasers of 254 µm length exhibited 5.5 mA threshold and 0.8 WA^{-1} slope efficiency with the 0.9 reflectivity on the back side, the 300 µm diameter half ring lasers showed 6.8 mA threshold and 0.33 $W\ A^{-1}$ slope efficiency as shown in **Figure 61.**

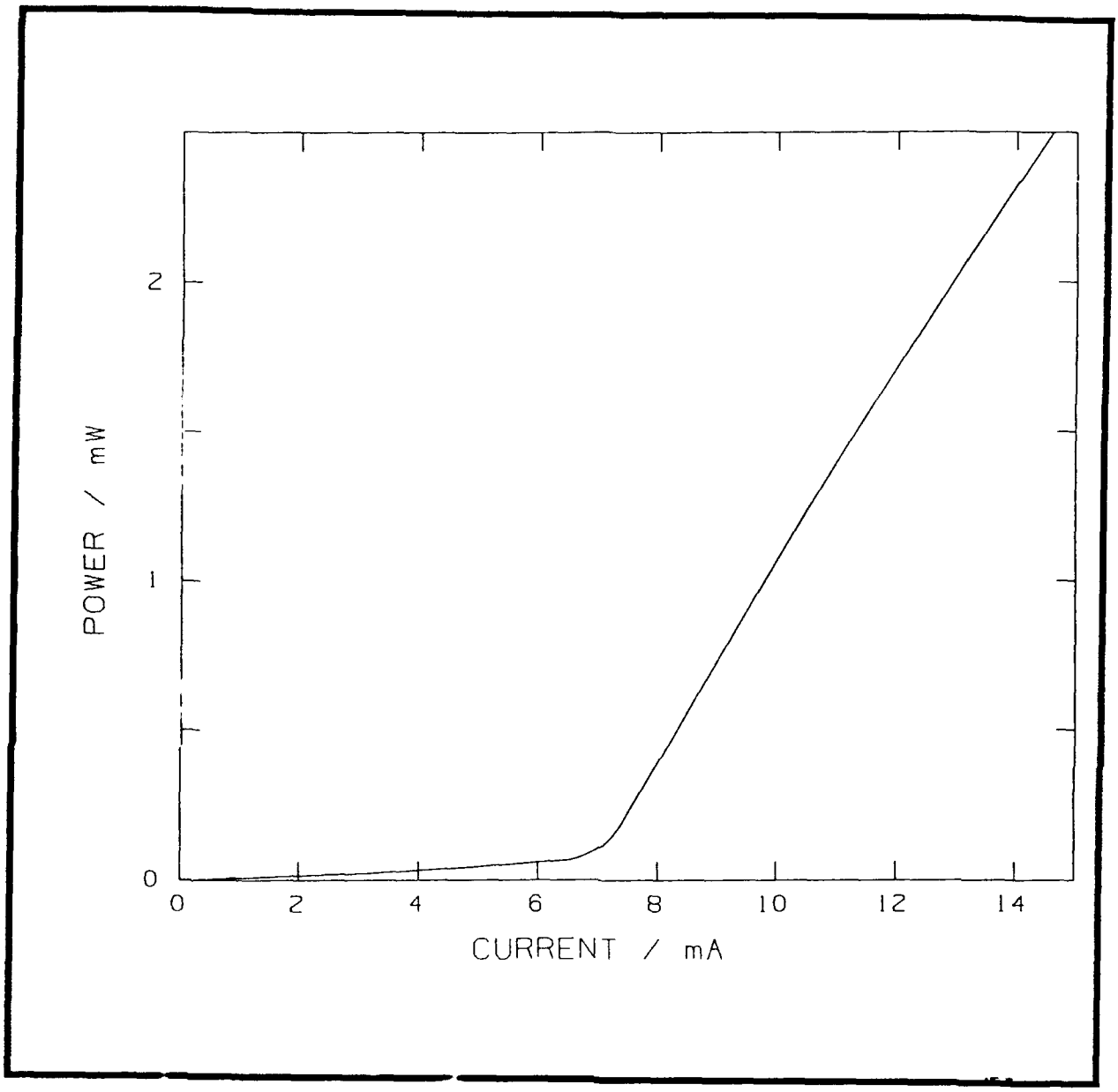

Fig. 61 The light output versus pump current input characteristic of the coated half-ring lasers operated cw with radii of curvature of 150 μm . The threshold is 6.8 mA and the slope efficiency is 0.33 W A^{-1} when light from both ends is measured.

The most important conclusion is that the **threshold current density per length** of the half circle laser (14.5 A m^{-1}) is lower than that of the straight laser (21.5 A m^{-1}). The reference laser has output coupling (due to the facets) equivalent to 26 cm^{-1} and approximately 9 cm^{-1} internal losses (assuming an internal quantum efficiency off 0.8). This allows us to put an **upper limit of 19 cm^{-1} on the distributed losses in the curved buried heterostructure** indicating that the losses associated with a radius of 150 µm in this single quantum well structure are **smaller than or equal to 10 cm^{-1}** in the best devices. Half rings with a radius of 100 µm performed less well, indicating that reducing the radius to this size is not a successful approach toward reducing operating current.

Uncoated lasers were tested for their small signal high frequency response. While straight lasers with 10 mA threshold showed 5 mA at -3 dB for 20 mA above threshold bias current, half circle lasers of radius of 100 µm and 150 µm both had threshold currents of 16 mA and -3 mA frequencies of 6.2 GHz and 4.5 mA respectively, indicating that the high frequency response is similar to straight lasers. **The higher frequency for the small radius is probably caused by the higher losses** and therefore larger operational gains of their active region.

In addition experiments were performed on full ring lasers. Since these devices do not exhibit any output coupler a highly

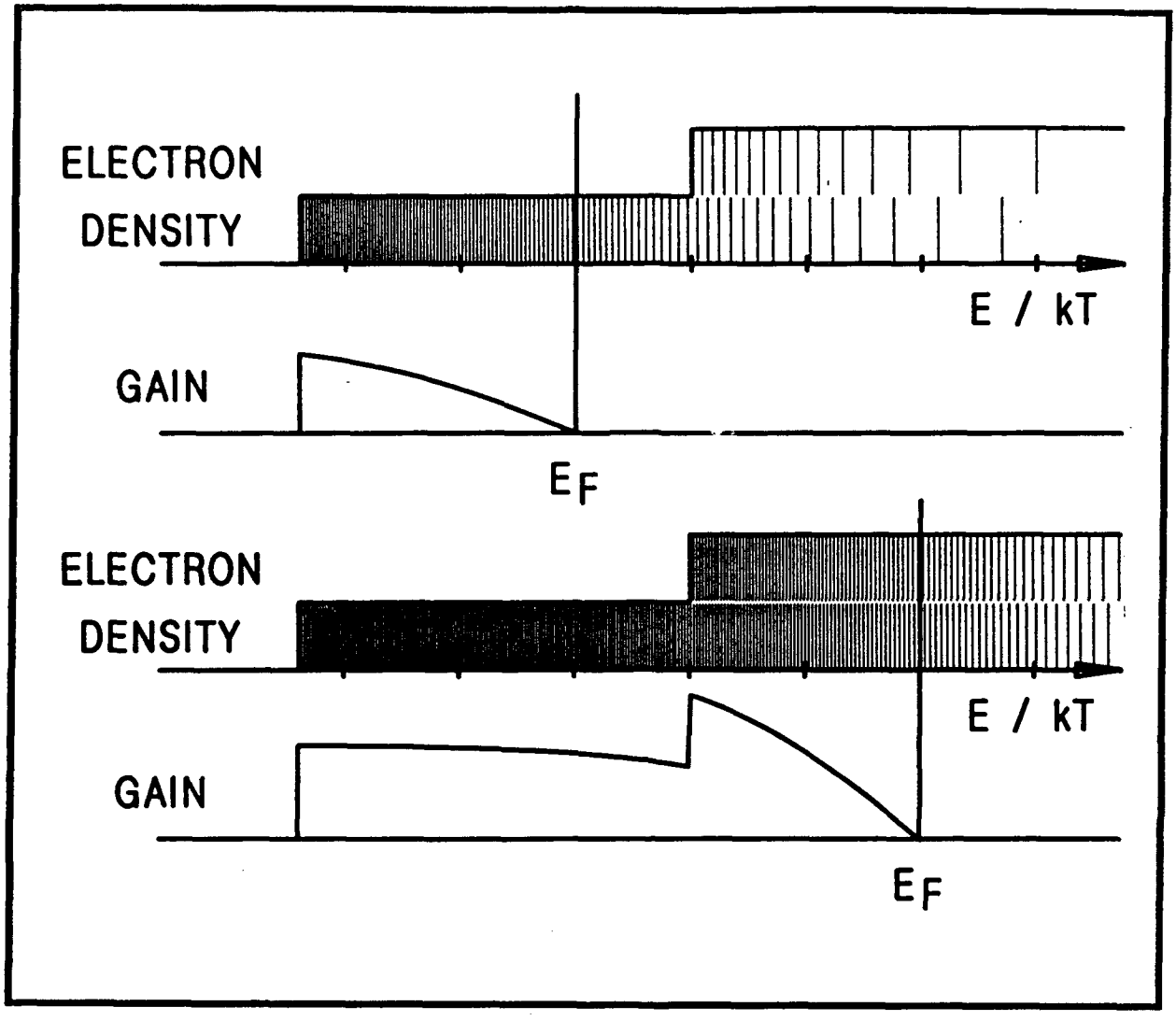

Fig. 62 Schematic diagram of the staircase like density of states as a function of energy. The shading indicates the occupation and the lower set of curves gives the associated spectral gain distribution. While (a) describes a moderate peak gain situation, (b) describes the case of high required gain and the maximum gain is obtained from the second quantized state.[1] The high occupation of states providing the wide gain spectrum is causing the threshold current density to be high in this case.

sensitive spectrally resolved detector system was utilized. The gathered stray light emerging from a facet cleaved to the vicinity of the ring - but not directly engaging it - was measured. Upon threshold a sharp transition from the below lasing spectral output of many longitudinal modes to the appearance of same lasing longitudinal modes was utilized to determine threshold.[1] Full ring lasers with a radius of 150 μm exhibited threshold currents as low as 16 mA.

6.2 Increase of Quantum Well Laser Threshold Current Density

As described in the presiding chapters and in the last section, buried heterostructure lasers are capable of very low threshold currents, especially when single quantum well structures are incorporated in well design resonators. However, if losses became excessive threshold currents increase very rapidly for single quantum well lasers.

The theoretical prediction indicates that the limited amount of modal gain available from the first quantized state transition is the fundamental reason for the sub-linear modal gain versus pump current density relation. The cause of the limit of available gain resulting from the density of states function is indicated in Figure 62 the result of a detailed modeling of the maximal modal gain versus pump current density is shown in Figure 22.

Moreover, the theoretically predicted **sub-linear** modal gain versus current density of single quantum well lasers shows **enhanced** in experimental findings. The reason may be increased optical losses with increased carrier density or reduced internal quantum efficiency with increased carrier density or both.

Consequently, the sub-linear modal gain versus pump current density relation is experimentally found to be very strong. Prove is found in the inability of narrow and deep single quantum well lasers, to be pushed to the second quantized state transition lasing, upon increasing the modal gain requirement, if the material and fabrication of the device are inferior. The laser takes very high current densities, however, its active region does not produce high modal gain.

The implication of these single quantum well laser properties is that **degradation of device performance is rapid with moderate increase of internal losses due to fabrication or design difficulties.** Fortunately there is an independent means of measuring this undesirable operational condition. This is important, because the threshold current may be high due to leakage currents or other external (to the active region of the laser) conditions. For a single quantum well active region to provide increased modal gain requires increased carrier density with in turn increases the band filling substantially and causes

a shift of the lasing wavelength.[1,2] This shift, as measured against reference lasers of the same material, can be as high as 20 nm, which is in almost all cases far beyond shifts due to material non-uniformities. In same cases the spectral shift associated with the transition to the second quantized state transition can be observed, which - depending on the width and depth of the quantum well - can be substantially lager.

If the fabrication especially of advanced structures like ring lasers is not of highest quality and increases the internal losses, the lasers threshold is drastically increased. The ring structure in particular is very demanding. The control of the width is not only important for the overall size of the active region but determines the lateral wave-guiding properties which in turn determine the bending losses. Furthermore the ring laser incompasses a variety of crystallographic direction which strongly effect the wet etching properties regarding the profile and possibly the roughness of the surfaces.

The regrowth involved in the fabrication of the buried laser structure depends on the quality of these surfaces with regard to the imperfection which cause optical losses as well as leakage currents. We had to conclude that at this point in the development of the buried structure single quantum well ring

laser we cannot control these sources of optical losses sufficiently to proceed with the integration of additional processing steps to incorporate grating output couples.

6.3 Buried versus Ridge Wave-guide

In light of the conclusion of the previous section an alternative lateral wave-guide structure was to be investigated. The structure chosen is the **ridge wave-guide structure.** Rather than replacing the material at the side of the active region by means of material removal and subsequent regrowth of new semiconductor material, the ridge wave-guide structure utilizes only removal of material.

The simplest way of describing the guiding effect is to consider the change of the **''effective index''.** The effective index is the Eigen value of the one dimensional index profile in the vertical structure that guides the mode. It is assumed that the structure supports only one mode as guided, all other modes are far to leaky to allow build up of optical intensity due to gain in the active region. Commonly only the real part of the index is considered - the so called cold cavity situation - with no gain or loss solved for.

The **effective index as a function of lateral position** provides a profile which can be engineered to form a lateral wave-guide.

Practically this approach neglects the effects on the guided mode due to interaction of the lateral and traverse index distributions, but may still be a useful approximation.

If material from the upper cladding layer is removed the index of refraction of the semiconductor is replaced by the index of refraction of air or the new surrounding material. Commonly this produces a substantial reduction of the index resulting in a modified Eigen value as soon as the region of changed index is close to where the optical field in the original wave-guide was substantial. This single sided removal of material effectively pushes the Eigen function into the lower side cladding layer such that the original transverse optical guide becomes less effective in guiding the mode. The **Eigen value is reduced** and because this condition holds for the sides of the laser stripe **provides lateral guiding.**

Most significant is that the semiconductor-air interface provides a strong index step such that the **evanescent field** of the optical mode in the air is very small and thereby the intensity at the interface itself is low. Consequently possible **optical absorption due to surface states will be minimal.** This is in contrast to the buried structure, where the optical intensity at the interface of the regrown material is high and consequently any absorption at the location of the interface due to imperfections or surface states provide significant

losses to the guided mode. The advantage of **lower losses** due to the interface/surface states of the ridge wave-guide structure together with the reduced processing complexity make the ridge wave-guide an attractive structure.

On the other hand, the buried structure could be fabricated with an active region with of 0.7 to 1.5 µm while the ridge wave-guide structure needs to be substantially wider. Its increased width is necessary due to fabrication tolerances. The ridge wave-guide structure is - as explained - a non-planar structure and an opening on the top of the ridge in an insulating layer has to be provided. **This alignment becomes extraordinary demanding for ridges whose top it less than 2 µm wide.** It implies that the effective active region which is slightly wider than the top of the ridge is no less than 3 µm wide.

This increased width has two major consequences. First, the **active volume** of the device is **larger.** Second, the **bending losses** for the same radius of curvature are **increased.** The later means that more modal gain has to be provided to reach threshold. Consequently both factors increase the threshold current of a ring laser, however the structure may be fabricated more repeatable.

6.4 References

1. M. Mittelstein, Y. Arakawa, A. Larsson, and A. Yariv, "Second Quantized State Lasing of a Current Pumped Single Quantum Well Laser", Appl. Phys. Lett., Vol. 49, No. 25, pp. 1689-1691, 1986.

2. Michael Mittelstein, "Theory and Experiments on Unstable-Resonator and Quantum-Well GaAs/GaAlAs Lasers", Ph.D. Thesis, California Institute of Technology, Pasadena, CA, (March 1989).

7 RIDGE WAVE-GUIDE LASER FABRICATION

The fabrication of ridge wave-guide laser and the possible stop etch layer structure are presented as a means to produce more consistent lateral wave-guide structures. This lateral design is applied to the ring structure.

7.0 Abstract

The fabrication of ridge wave-guide laser is discussed. Concern is concentrated on reproducibility and the stop etch layer concept is introduced as a means of achieving small variations in the guiding parameter of ridge wave-guides. Special attention is place on the consequences of this alternate lateral design on the curved wave-guide design of the ring laser and first results are presented

7.1 Ridge Wave-Guide vs Buried Heterostructure Fabrication

Similar to the buried heterostructure the ridge wave-guide structure depends on etching a pattern for lateral guiding vertically into the stack of layers provided by a first growth.

The buried heterostructure requires a very narrow mesa of 1 to 1.5 μm width at the height of the active region. Wider structures do not suppress multi-mode operation unless the second growth which buries the mesa, is very closely matched in material

composition (in our case Al-concentration) to the first growth material. The very tight requirement is difficult to achieve with the very deep etch performed (typically 4 µm in our case). With straight lasers only one crystallographic orientation is encountered, but for the ring structure **different crystallographic orientations are an inherent complication.** While the narrowness of the active region and the wave-guide is theoretically advantageous for small radius bends, the experimental finding indicates no lasing for the tested 50 µm radius devices. The theoretical advantage is only realized if the wave-guide is narrow in **all the orientations** appearing in the resonator, if in some orientations the width is exceeding the limit the ring resonator becomes leaky and low threshold lasing from a single quantum well active region is not achieved.

The ridge wave-guide structure, in contrast, relies on a shallow etch, 1 to 1.5 µm deep. This material removal results in a modified vertical wave-guide such that an effective real lateral wave-guide is established without subsequently material deposition. A more in-depth treatment should utilize a two-dimensional approach because the interaction of the transverse and lateral effects. In any event, the resulting structure does not utilize a second regrowth and therefore has the potential to be realized with higher reproducibility. Typical sizes of the mesa structure are 2 to 5 µm width at the top of the mesa. The advantage of this structure is that the

three-fold reduction in etching depth results in a approximate three-fold reduction in the orientation dependent width of the etched structure. The results obtained regarding this parameter are described in the next paragraph. The vertical etching in the ridge wave-guide structure is carried close to the active region. The distance to the active region in the order of 0.2 to 0.5 µm has to be obtained with high precision for reproducibility. The experimental approach chosen is described in the next section.

7.2 Ridge Wave-guide Structure, the Experimental Approach

The experimental approach to investigate ridge wave-guide laser structures was based on **two sets of experiments.** On one hand, a stop-etch layer technique was utilized to implement built-in high degree of control on the processing and on the other hand, a simple single etching was performed using a set of etching times to select the optimum etch depth afterwards.

The **stop-etch layer technique is based on a modified vertical structure** provided by a special wafer growth. The modification is an additional layer introduced so that the overall properties of the optical wave-guide are compromised minimally. Broad area lasers were fabricated to verify the material quality. Within the variations of devices, the material matched the properties of our standard material. Hence, no significant

degradation occurred. A properly designed process allows us to use the additional layer to slow-down the etching speed when performing the vertical etch. Consequently, the surface to which the etch is to be performed is planarized. More importantly, because the depth at which the etch stops (or slows down) is controlled by the layer structure. **Reduced sensitivity with regard to the possible variations of layer thickness of the material to be removed is obtained.** In our case, the structure incorporates a 0.1 Al-content layer of 0.1 μm thickness placed 0.3 μm above the active region. This layer is about 1.3 μm below the original top surface of the structure such that the total structure is from top to substrate as follows.

0.2 μm	p^+-GaAs	contact layer
1.1 μm	p -$Ga_{.5}Al_{.5}As$	upper cladding layer
0.1 μm	p -$Ga_{.9}Al_{.1}As$	stop etch layer
0.1 μm	p -$Ga_{.5}Al_{.5}As$	upper cladding layer
0.2 μm	p -$Ga_XAl_{1-X}As$	graded region X=0.5->0.2
75 Å	i -GaAs	active layer
0.2 μm	n -$Ga_XAl_{1-X}As$	graded region X=0.2->0.5
1.5 μm	n -$Ga_{.5}Al_{.5}As$	lower cladding layer
100 μm	n^+-GaAs	substrate

A conventional etch is utilized to etch close to the stop etch layer without actually reaching it. Then a highly selective

etch that we have developed previously is used to remove the remaining material above the stop etch layer. **Even extended etch times do not result in penetration of the stop etch layer.** As a result, the structure exhibits a remaining layer thickness above the active region of uniform thickness determined mainly by the original growth of the layers and very little by the actual etching process. Actually, the process is more involved: The top most layer, which is the contact layer, is GaAs which is not etched by the selective etch. If no selective removal is performed, this layer will be undercut and the overhanging material will make top contact metallization difficult. Consequently, we performed three etch steps utilizing two photoresist masks for the stop etch layer process. Also the width of the ridge wave-guide was varied and very narrow up to about 6 µm wide ridges were fabricated for subsequent investigation.

As an alternative approach a simple ridge wave-guide process was investigated. In this case, the a single photoresist masking step and a single etching step was used. In preparation, the time-dependent etch-depth was determined on small test pieces of the wafer. Then the remaining wafer was divided in three pieces, one of which was etch at the previously determined optimum time, the other two where etched **slightly shorter** and **slightly longer** respectively. Thereafter, lasers made from material of all three etch times were investigated.

7.3 Straight Wave-Guide Laser Fabrication

The experimental findings are similar for the best devices of both runs. Threshold currents for 1000 µm long devices are near 35 mA and the slope efficiencies for uncoated devices reached 0.45 . With both methods we are able to fabricate good ridge wave-guide lasers, however, for the simple method we wasted two thirds of the material. Actually the etch time considered optimum resulted in the best lasers. The longer etching time resulted in less favorable far field pattern, as expected for to strong of a guide. The results regarding the width of the ridge which was varied in the stop etch layer experiments indicate, that near 4 µm width gives the best far field pattern. Consequently our 5 µm width ridge wave-guide lasers from the simple etching experiment are wider than optimal.

However, the thorough investigation of ridge wave-guide structures revealed that variations in the etch rate are such that use of etch time to control etch depths for ridge wave-guide laser structures is not practical for reproducible device fabrication in our laboratory.

7.4 Ridge Wave-Guide Ring Structure Investigation

In order to see if the etching process qualifies for ring structure ridge wave-guide fabrication etch test were performed

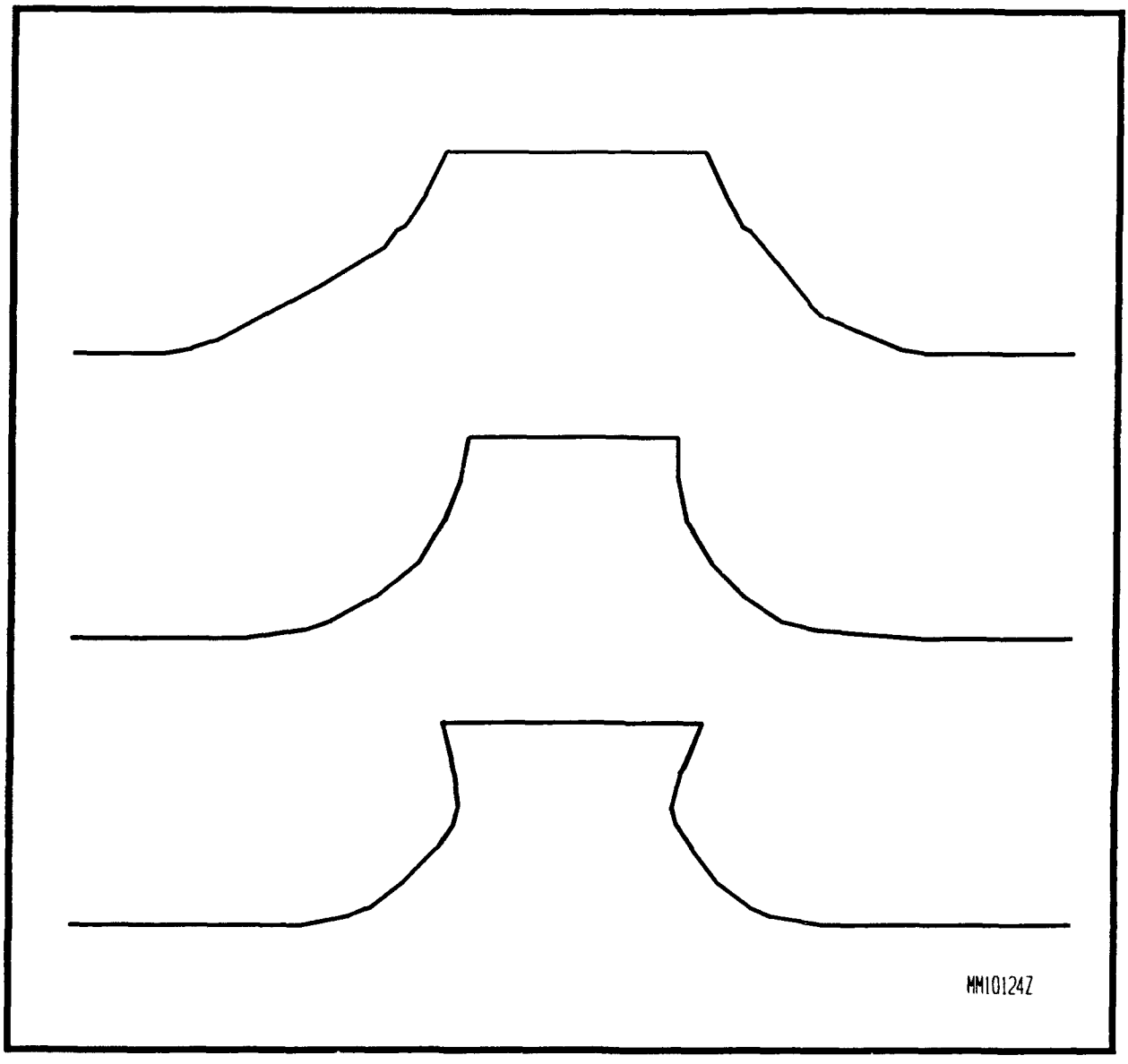

Fig. 71 Cross-sections of ring ridge wave-guide test structure scaled to 12.500 X magnification as taken from SEM pictures. The [0 $\bar{1}$ 1] at the top shows the V-groove characteristic. The [0 0 1] at the middle was obtained form braking the chip. The [0 1 1] at the bottom exhibits up to 0.35 µm overhang characteristic for the dove-tail orientation.

and investigated. The etching depth was increased in order to enhance the variation caused by the different crystallographic orientations. Starting from a 8 µm wide SiO_2 mask a ring mesa with a width at the top of 2.5 µm to 3.1 µm was obtained. The measurement was performed in a SEM to obtain high relative accuracy and resolution. This +-0.3 µm variation is expected to be reduced to +-0.2 µm if the etching time is scaled for ridge wave-guide fabrication. Test structures were cleaved in the two perpendicular directions and broken in the intermediate direction to investigate the cross section of the mesa as shown in **Figure 71.** The preliminary finding looked very promising in that the profile seen in the SEM exhibits little of the undercutting usually obtained in the dove-tail direction and small variation of the width of the ridge. The overhang is no more than 0.35 µm and negative slop region is limited to the to 1.0 µm of the etching depth. The total etching depth of this test was 2.4 µm an increase of more than 50% of the typical etch depth for ridge wave-guide structures. This increase was used to enhance the effects and ease observation. The optical mode has very little intensity at a location 3/5 up from the bottom of the ridge wave-guide etching depth so that the observed structure is satisfactory. This is a significant finding, because the undercut is not only creating problems for the contact metallization but increases the losses for the guided optical wave.

7.5 Ridge Wave-guide Processing

The method utilizing a stop etch layer has been refined and the processing recipe has been developed. Photoresist stripe pattern on SiO_2 is under-etched in buffered HF to the desired widths. This allows for experimental variations of this parameters. The full width of the SiO_2 mask of 5.5 μm has shown good results. A H_2SO_4:H_2O_2:H_2O etching solution (Sulfuric Acid : Hydrogen Peroxide : Water) of 1:8:40 composition is cooled in a water/ice bath and used for 120 seconds to non-selectively etch into the GaAs/GaAlAs layer structure approximately 1.1 μm deep. A proprietary etching solution is heated in a water bath to 64°C and used for 120 seconds to selectively etch GaAlAs with Al concentrations higher than about 0.2 . This etch removes approximately 4000 Å cladding layer material of Al concentration between 0.4 and 0.6 . It effectively stops at the stop etch layer 1.3 μm below the original top surface. A NH_4OH:H_2O_2 etching solution (Ammonium Hydroxide 30% : Hydrogen Peroxide 30%) of 1:24 composition is utilized at laboratory temperature for 15 seconds to remove the overhanging GaAs contact layer with very little etching of the stop etch layer and cladding layers. The resulting ridge exhibits about 5 μm width at the bottom and 3.5 μm at the top when etched such that the laser ridge wave-guide exhibits a V-grooved pattern in cross section that is the case of the ridge alined in the (0 $\bar{1}$ 1) orientation.

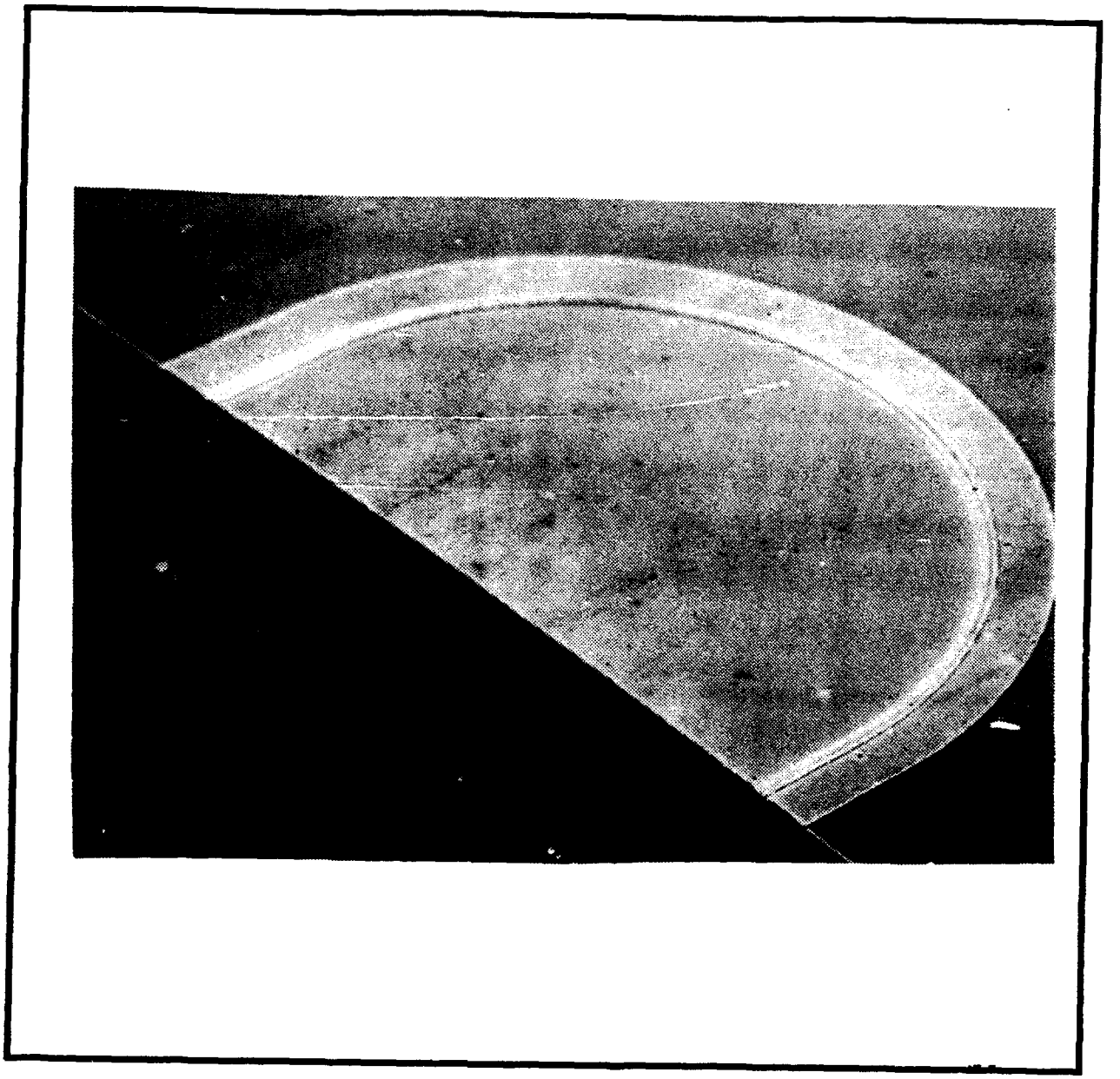

Fig. 72 Perspective SEM view of half-ring ridge wave-guide laser. The ridge is the narrow elevated region close to the outer etch of the top metal (showing bright in the picture).

7.6 Multiple Quantum Well Ridge Wave-guide Ring Laser

In a experimental approach lasing from ridge wave-guide laser structures of half ring structure was achieve. In order to boost the available gain a multiple quantum well structure otherwise similar to the structures described previously was utilized. This approach was chosen to succeed with lasing even if the low threshold cannot be achieved. The ridge wave-guide was etched very close to the active regions (the quantum wells) leaving only about 0.15 μm of the graded region of the optical wave-guide. The width of the ridge at the top was close to 2.5 μm and the radius of 150 μm was utilized for the half-ring laser.

The devices lased at room temperature, however, threshold currents were high at 130 mA. This proves the concept, that ridge wave-guide lasers can use multiple quantum wells as gain medium in ring laser structures. In **Figure 72** a half-ring ridge wave-guide laser is shown. The metallization extends from the inside slightly beyond the ridge. The ridge is visible mainly due to the sharp contrast the sloped side walls produce even so they appear very tiny in the figure. The dark lower left region is the single cleave of the crystal that forms both end mirrors.

8 GRATING FABRICATION

The fabrication of the gratings is described. The facility to achieve gratings, however, is described in the following chapter. In all cases of interest for this research and development effort gratings are fabricated on the top surface of semiconductor wafers. Holographic exposure is transferred from thin photoresist into the semiconductor by chemical etching. The main work concentrated on operational conditions to accomplish definition of grating near raised structures in order to avoid otherwise necessary additional regrow as described in chapter six.

8.0 Abstract

Fabrication of gratings with a period near 2500 Å on planar and non-planar surfaces are described. The production of second order Bragg reflector is depictured.

8.1 Surface gratings

Initially substrate material with **fully planar surfaces** were utilized. A specially formulated high solvent contend photoresist is span on. Evaporation leads to a approximately 300 Å thick photoresist layer which is pre-baked for preparation of the exposure. Carefully controlling the exposure dose for **near one third opening** of the photoresist after development produces the best results for the subsequently etched grating.

The grating is etched into the semiconductor material in a low concentration etch at lab temperature for depth in the range of 100 to 500 Å as confirmed by high resolution scanning electron microscopy (SEM). Depending on semiconductor orientation, fraction of the photoresist opened, and depth of etching the grating shape varies from close to **rectangular** via nearly sinusodial to **triangular** ridges elevated over a plane base. The uniformity proved to be mostly determined by the photoresist. Any contamination or vibration during the spinning causes **severe** non-uniformity in photo resist thickness that transform into enhanced non-uniformity in the grating. Also the **etches of the wafer produce strong disturbance of the photoresist flow** upon spinning, so that only a roughly circular central part of the wafer turns out to be useful for grating formation. This restriction asks for square or more round wafers to reduce waist; larger sizes provide an increased fraction of useful area. An alternative might be spray deposition of the photoresist as a means of less sensitive deposition process, but it was not experimented width.

8.2 Fabrication of Grating on Non-Planar Surfaces

The ability to fabricate surface gratings on a **non-planar** structure enables the grating fabrication of a **vertical emitter after the active part of the laser structure has been completed.** The significance is described in the section 3.5 of this report. Achieving grating fabrication on a non-planar surface, allows

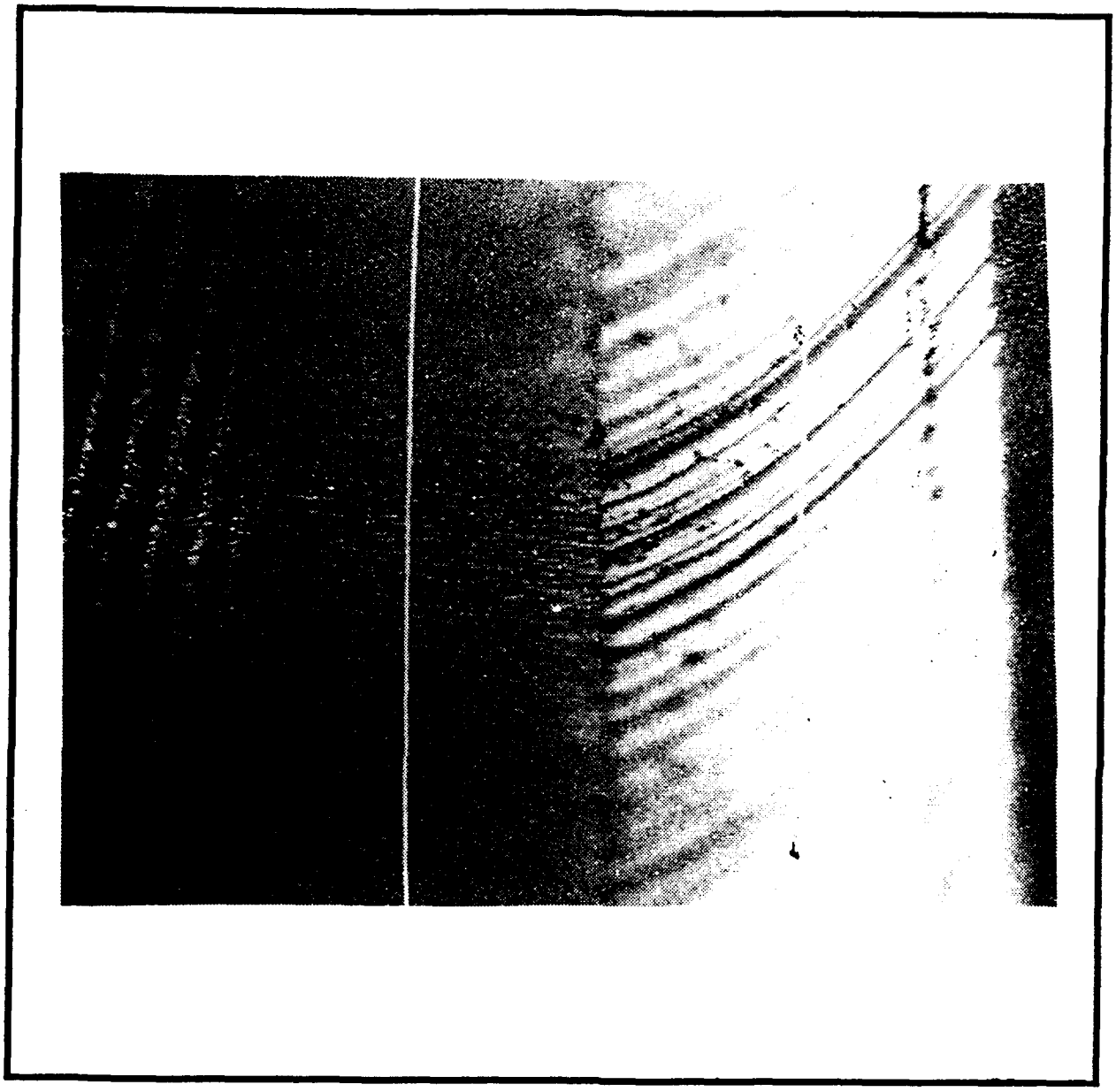

Fig. 81 SEM of etched grating (left) next to simulated active region of ring laser (right) showing the short transition region.

an uninterrupted growth of the active region of the laser. This greatly reduces the risks in research and development of the fully integrated vertically emitting ring laser.

In order to demonstrate the capability to produce suitable gratings, non-planar substrates were fabricated to simulate the conditions to be expected in laser fabrication. Several methods of preparation for grating definition were investigated and it was found that a tolerable transition zone of width less than 5 μ can be achieved. The small transition zone exhibits no grating. The grating starts rather abruptly at the end of the transition zone without defects. In Figure 81 the experimental result is illustrated. The SEM photo shows on the right the elevated region simulating the structure embedding the active region of a laser. Towards the center of the figure the vertical step is evident, its height is the upper limited considered for laser fabrication. The left hand side of the figure shows the fabricated grating, its orientation is tilted with respect to the step to demonstrate the abruptness of the onset for the grating. In the center the transition region is evident. A little bit of transition region is beneficial because partial blocking of the upwards emitted light by the step would cause reduced smoothness in the far field of the vertically emitted beam. In Figure 31 the considered overall laser structure was

Fig. 82 SEM cross-section shows a grating etched near an 0.75 μm high step in the (0 1 1) orientation starting within 3 μm of the step.

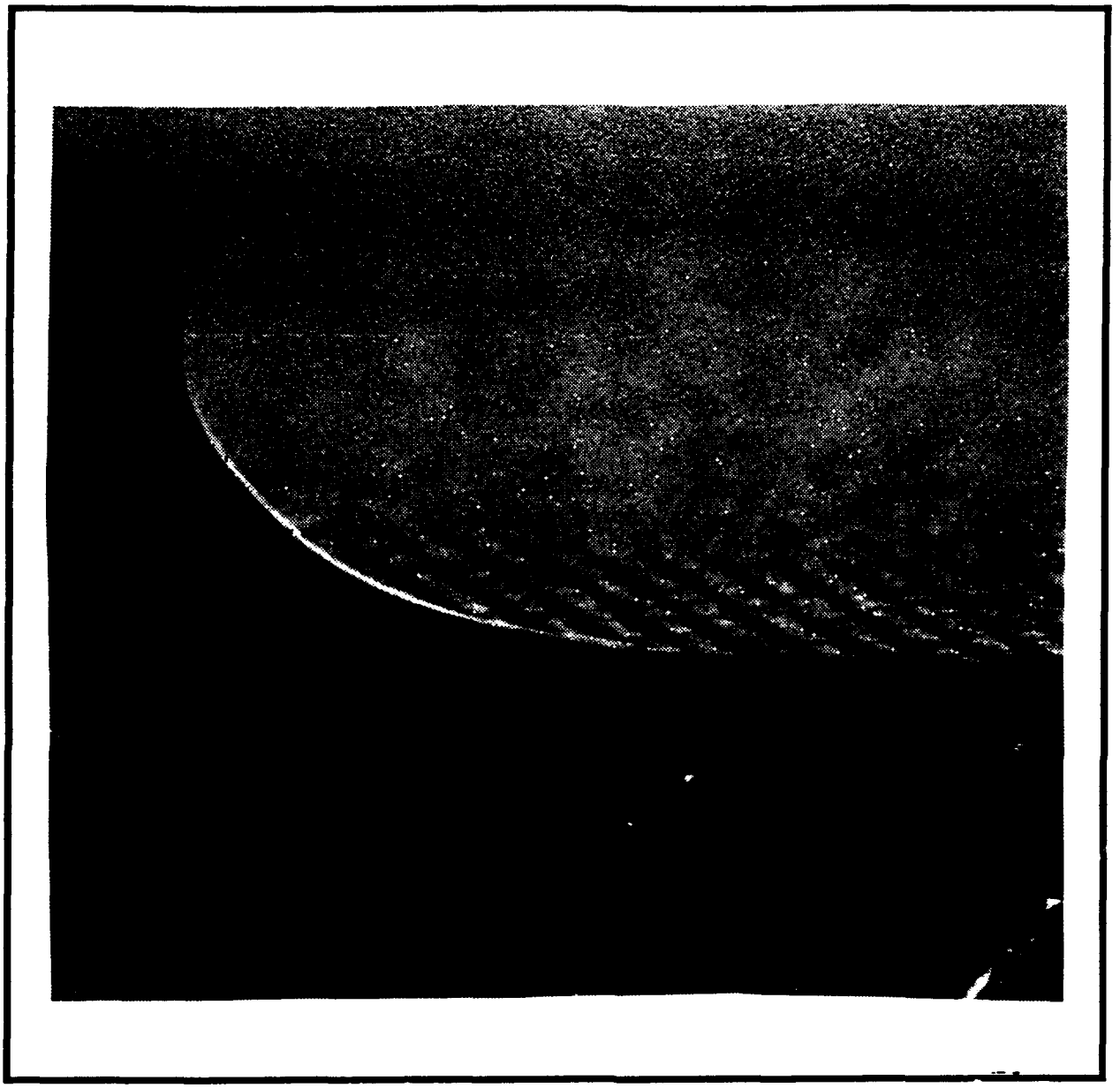

Fig. 83 SEM cross-section shows a grating etched near a step of 1.8 μm height. In this case the grating starts immediately at the lower end of the slop of the step which is in the $(0\,\bar{1}\,1)$ orientation.

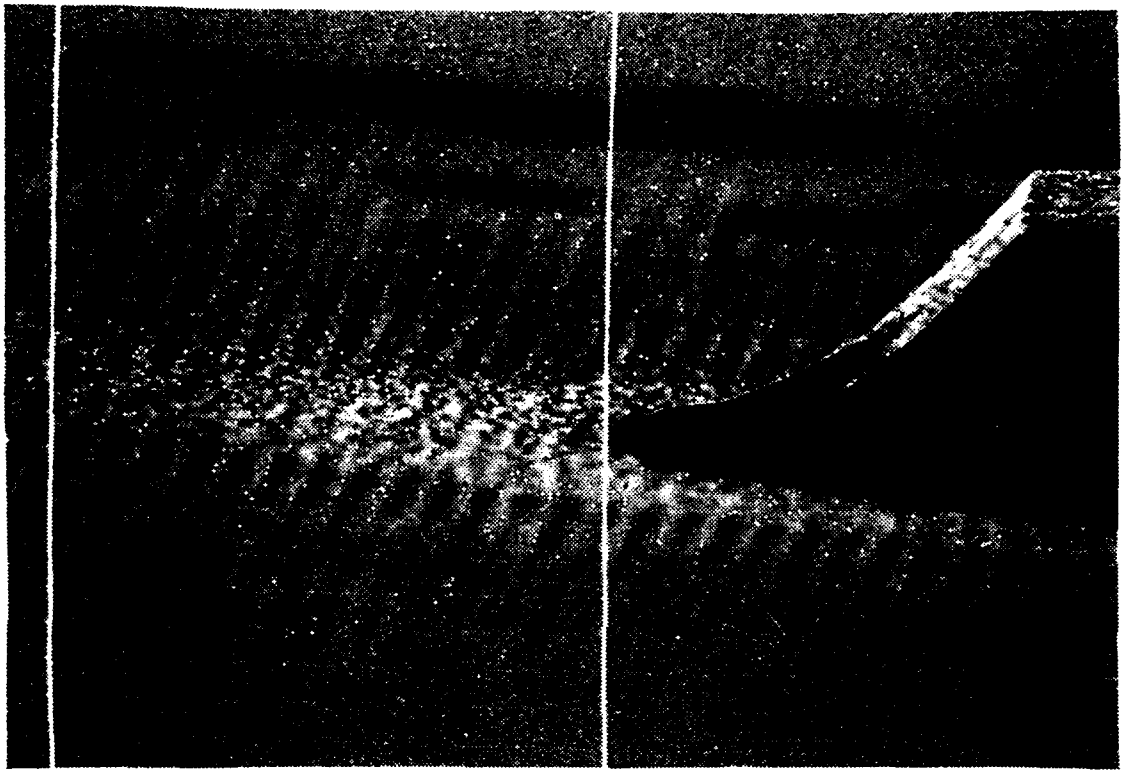

Fig. 84 SEM perspective of the end of a ridge in the (0 1 1) orientation. The grating formation is spaced 3.2 μm from the bottom of the slop as indicated by the markers. This photo shows a smooth transition of the ridge wave-guide into the grating region.

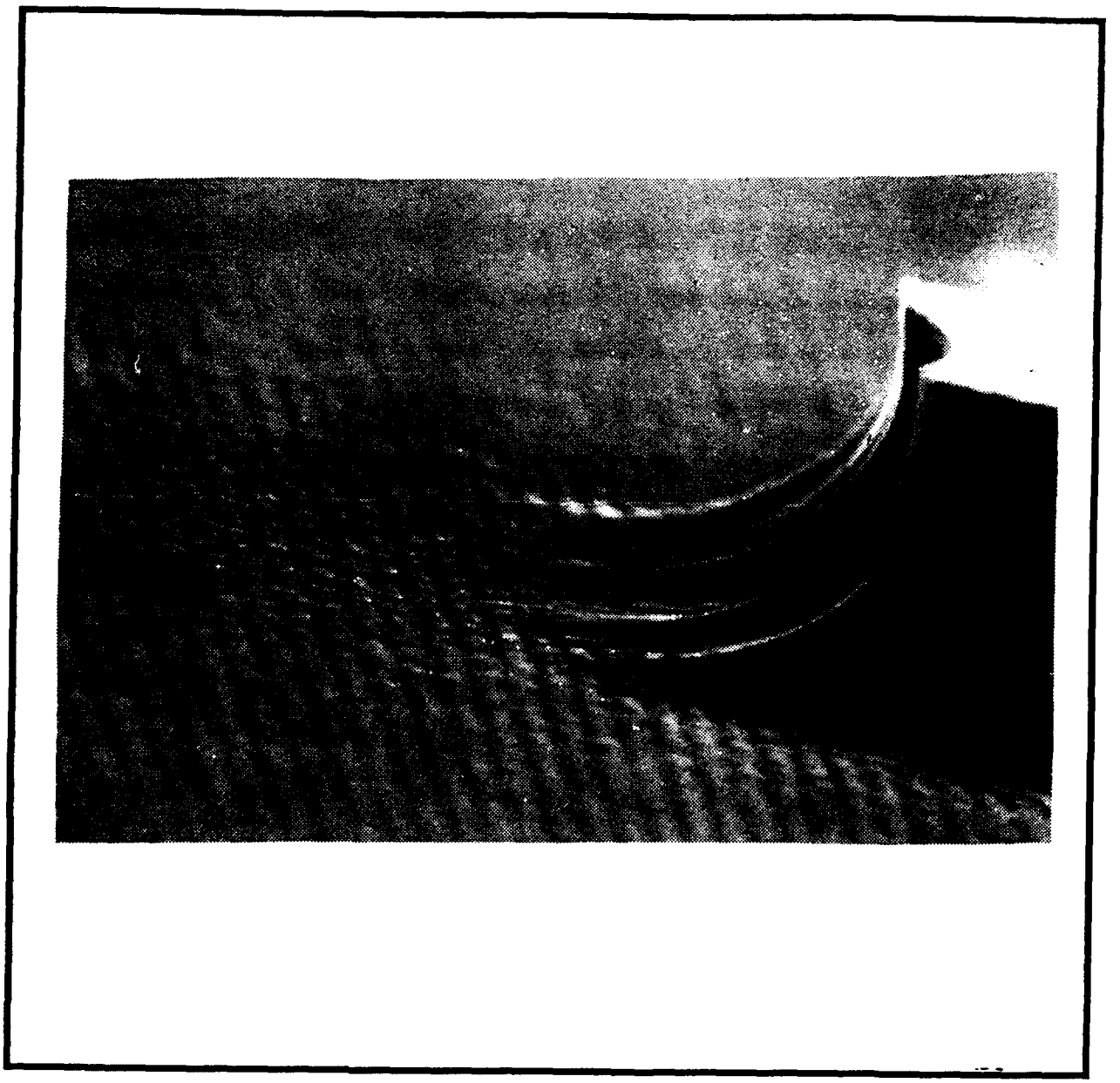

Fig. 85 SEM perspective of grating formation abruptly a the end of a ridge test structure which is orientated along the $(0\,\bar{1}\,1)$ direction.

shown. The otherwise planar surface exhibits a "hole" whose bottom is the grating. The figure is not to scale, the real design appears nearly flat.

More investigations on gratings near wide stripe ridges were performed. In **Figure 82** a [0 1 1] cross-section shows a grating etched near an about 0.75 µm high step along the (0 1 1) orientation starting within 3 µm of the step. In **Figure 83** a cross-section shows a grating etched near a step 1.8 µm high. In this case the grating starts **immediately** next to the slop of the step which is in the (0 $\bar{1}$ 1) direction.

Subsequent investigations were concentrated on **narrow stripe ridges the shape of ridge wave-guide single lateral mode lasers.** In **Figure 84** the end of a ridge in the (0 1 1) orientation is shown where the grating formation is spaced 3.2 µm from the bottom of the slop as indicated by the markers. This photo shows a smooth transition of the ridge wave-guide into the grating region, however, the orientation of the crystal is unfavorable for the ridge wave-guide laser formation. In **Figure 85** grating formation abruptly at the etch of the ridge is shown. The end of the ridge which is in the (0 $\bar{1}$ 1) direction does not show a good surface however.

In the last figure in this selection a top view of the end of a simulated ridge wave-guide laser is shown. The strip mesa

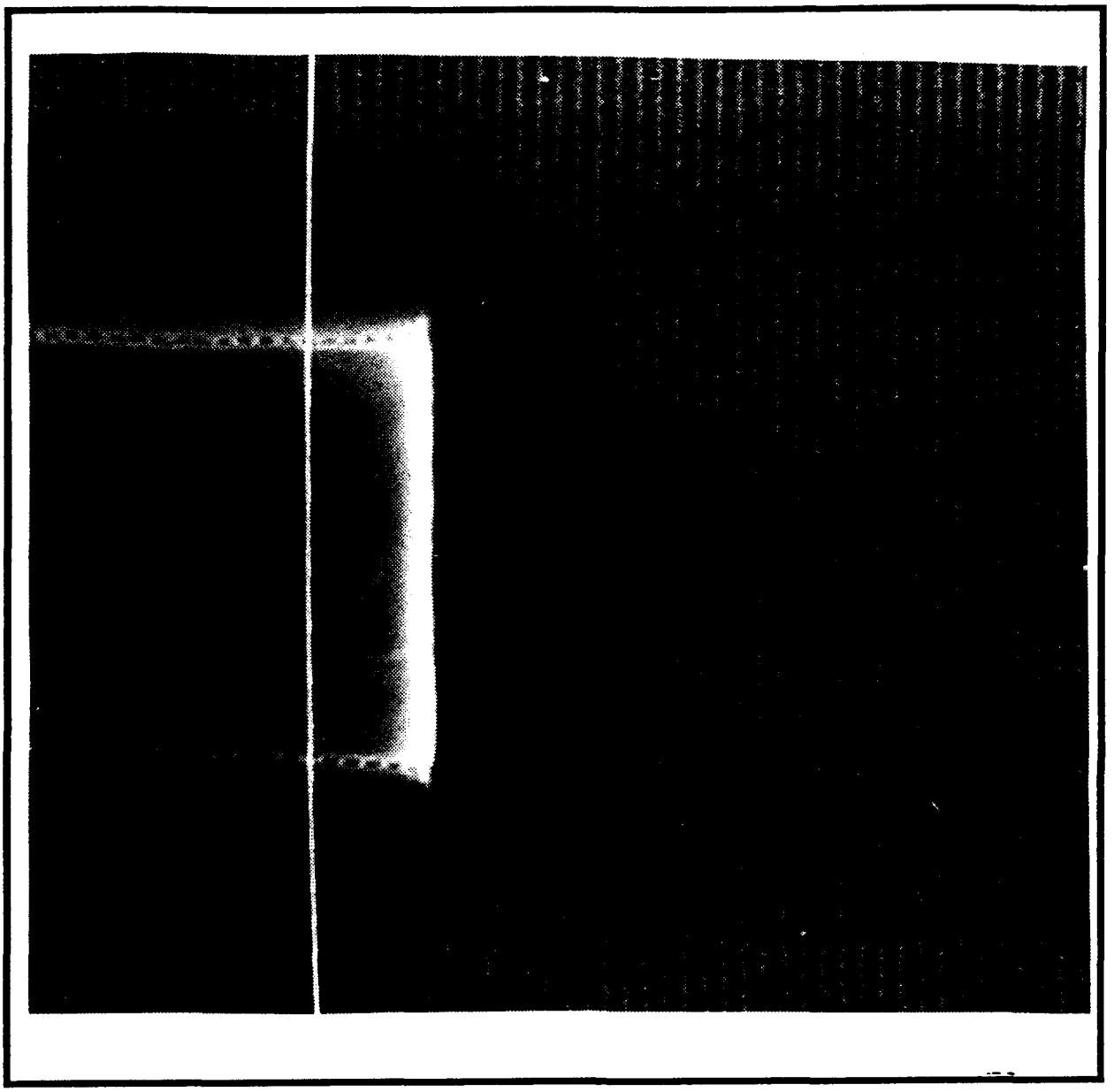

Fig. 86 SEM top view of strip mesa same 5.5 μm wide and a grating with a 2500 Å period. The white line is a marker which was used to determine the grating period.

is 5.5 µm wide and the grating has a 2500 Å period (**Figure 86**). These figures indicate a variety of options for the grating formation and are very encouraging for the integration of gratings and lasers.

8.3 Vertical Output Grating Coupler

To demonstrate performance parameters of vertical emitting lasers first straight devices with second order gratings on the semiconductor surface have been fabricated. This is based on our successful demonstration of "fabrication of gratings on non-planar surfaces" described in the presiding section of this report. The ridge wave-guide lateral structure is very similar to the described longitudinal integration of a surface grating for vertical emission since the top material is etched out to the same depth.

Continued investigation of grating fabrication in particular on non-planar substrates has been performed. Initial strong non-uniformity require a closer investigation. Two dimensional mesas to simulate conditions of ridge wave-guide distributed Bragg reflector lasers were fabrication. Even though these structure are less than 1.5 µm high, they have a strong effect on the spinning of the photoresist/thinner mixture spun on at high speeds. As a result, the photoresist thickness depends on the position with respect to the center of the spinner and therefore, orientation of the laser with respect to the radial

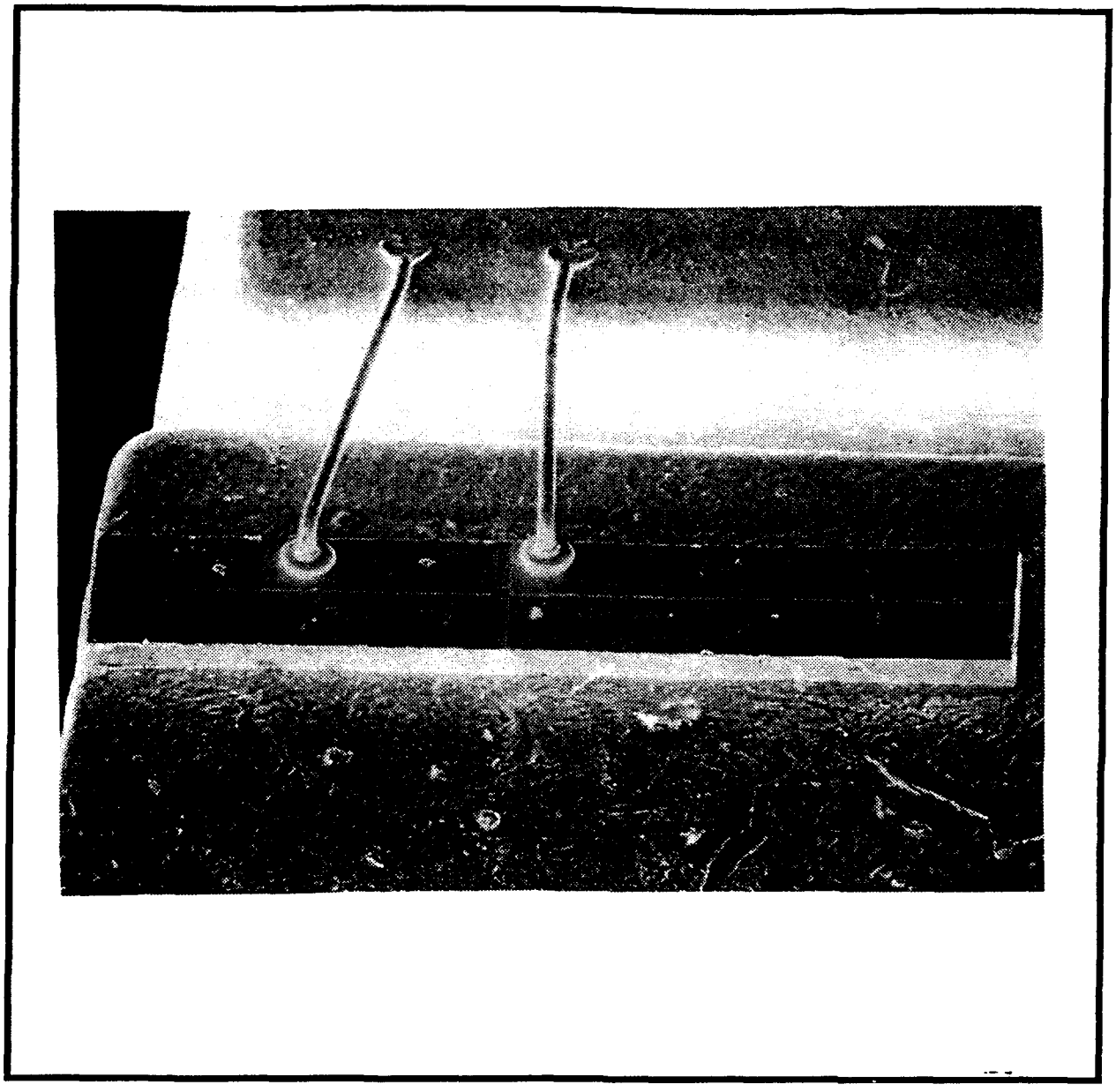

Fig. 87 SEM perspective view of a mounted vertical emitting laser. Shown as a small dark area is the grating region near the middle of the picture. The trench across the chip interrupts the metallization and exposes the grating. Two wire bonds are used to provide current to the two active regions.

direction during the spinning process. Compromise conditions were found to get acceptable grating definition in the photoresist upon holograph exposure. After baking the grating in the photoresist it is transferred into the GaAlAs by etching for 20 seconds in a H_2SO_4:H_2O_2:H_2O solution (Sulfuric Acid : Hydrogen Peroxide : Water) of composition 1:8:285 at laboratory temperature. The resulting grating in the GaAlAs is about 500 Å deep. The depth is reproducible as verified by scanning electron microscope (SEM) investigations. For thinner photoresist, the grating can be extended right up to the lower slope of the mesa.

Distributed Bragg reflector ridge wave-guide lasers have been fabricated. A 950 µm long active region is directly coupled to a 500 µm long second order retro-reflecting grating. Initial testing indicates lasing. Subsequently a structure with features closer to the integrated vertical output coupler for ring lasers was investigated. The test devices were 1700 µm long of which a length of 25 µm was etched down close to the active region and a 0.25 µm period grating was holographically defined and then etched in to the stop etch layer.

In **Figure 87** a mounted device is shown. The vertical emitting laser chip shows the grating region as the small dark area near the middle of the picture. The top surface of the chip appears uniformly medium dark apart from the side wall of the ridge which appears as a white line all along the chip. Two wire

bonds are used to provide current to the two active regions one on each side of the grating. The trench that separates the two parts of the top metallization and exposes the grating is clearly visible being orientated across the chip.

Mounted devices were installed in the new **test facility** and far field scans through the vertical output orientation were performed. The devices did exhibit apart from the strong facet emission a **well defined angular narrow emission.** This emission was investigated in the longitudinal and transverse far field direction and identified as coming from the grating. The grating seamed to influence the laser only weakly and did not define the wavelength of the devices. Consequently two directions of emission symmetric to the vertical were observed which we associate with the **individual emissions from the two counter-propagating beams inside the wave-guide.** The far field distribution exhibited an aspect ratio of about 1 to 4 with the wider angle transverse. This is the predicted signature of the grating whose illuminated part is narrower (transverse) than its length. The grating should be placed closer to the active region in order to increase the fraction of light that is coupled out via the first order of the Bragg grating.

9 GRATING FABRICATION FACILITY

The set ups and facilities utilized to produce the gratings described and depictured in chapter 8 are described. The claim for the novel grating facility invented for this research and development effort is presented.

9.0 Abstract

The method of holographic fabrication of surface gratings is presented. The requirements for this research and development effort are analyzed and the design of a novel arrangement for holographic grating fabrication with different periods is described.

9.1 Introduction

Facilities for holographic grating fabrication usually let two internal extended beams interfere on a target surface. The interfering beams expose a thin layer of photoresist for subsequent processing. The grating pattern is obtained by the interference of the two beams impinging on the surface with different angles but a common polarization component. Even though two arbitrary angles of incidence can be considered, the following description is restricted to the symmetric case where the two angles are in the same plane and equal magnitude and opposite signs are specified. Furthermore, S-polarization is considered to obtain an

interference term for all incidence angles. In this case, the holographic grating period l for the angle of incidence α in the medium with index of reflection n is $l = \lambda/(2n \sin(\alpha))$.

To vary the grating period for fixed λ and n the angle of incidence has to be changed. To insure good coherence, the two internal beams are usually obtained from a single input beam by beam splitting. The use of equal optical path length is beneficial to reduce the required coherence lengths of the light source.

9.2 Test Setup and Evaluation

Following these general guidelines, a facility for holographic grating fabrication was set up. Individual post-mounted components were used and the target holder was mounted on a translation stage. Two mirrors for redirecting the internal beams are mounted on rotational stages which allows realignment of the system in order to facilitate generating gratings with period in the range of 0.2 µm to 1.0 µm.

Typical second order gratings for GaAlAs lasers exhibit a periods of 0.24 µm. The system consists of a Helium-Cadmium laser which emits light in the 325 µm UV line. The laser beam is spatially filtered and expanded. The collimated

beam and the mechanical set allows nearly one inch beam diameter. This **first system** was successfully used to demonstrate grating fabrication. Its limitation are mainly that several components have to be realigned upon changing the desired grating period. The **accuracy as well as reproducibility of achieving a desired grating period** is limited.

9.3 Requirements for Improved Grating Facility

Consequently, implementations of the requirement to reproducibly and accurately achieve the desired grating period were evaluated. **The challenge is to provide the means to accomplish the beams splitting, redirection and targeting such that the angle of incidence on the target can be varied with a minimum of adjustments and a simple structure.** The solution implemented at Ortel Corporation is disclosed in section 9.4 .

9.4 Concept of improved Grating Facility

The grating facility utilizes **four basic components for a symmetric optical set up.** At the input, a beam splitter creates two internal beams. Two redirecting mirrors, one for each internal beam, are utilized to cause the redirected internal beams to overlap in the target area. Hereafter the term **beam** refers to the **central ray of actually extended**

beams. Symmetry maps each one of the internal beams onto the other internal beam. All four beams, namely, the two internal beams and the two redirected internal beams, are in the same plane, which will be referred to as the **reference plane.**

The four beams form a convex four cornered polygon. The **apex** of the two internal beams is opposed to the target area. The symmetry point of the target area will be referred to as **target** point. The inclination of the redirected internal beams with respect to the normal of the target plane (i.e. the symmetry axis of the polygon) defines α were $0° \ll \alpha < 90°$. The inclosed angle of the mirrors and the target plane defines β were $45° + \alpha/2 < \beta < 90° + \alpha/2$. The enclosed angle of the two internal beams emerging from the beam splitter defines γ were $0° \ll \gamma < 180°$. Consequently, the desired angle of incidence on the target is $\alpha = 2(\beta - 90°) + \gamma/2$ and the required angle of the redirecting mirrors is $\beta = 90° + \alpha/2 - \gamma/4$.

If the angle γ and the distance of the apex to the target plane called D are **fixed**, then to change the angle α the **redirecting mirrors have to be rotated** (β) **and moved** to

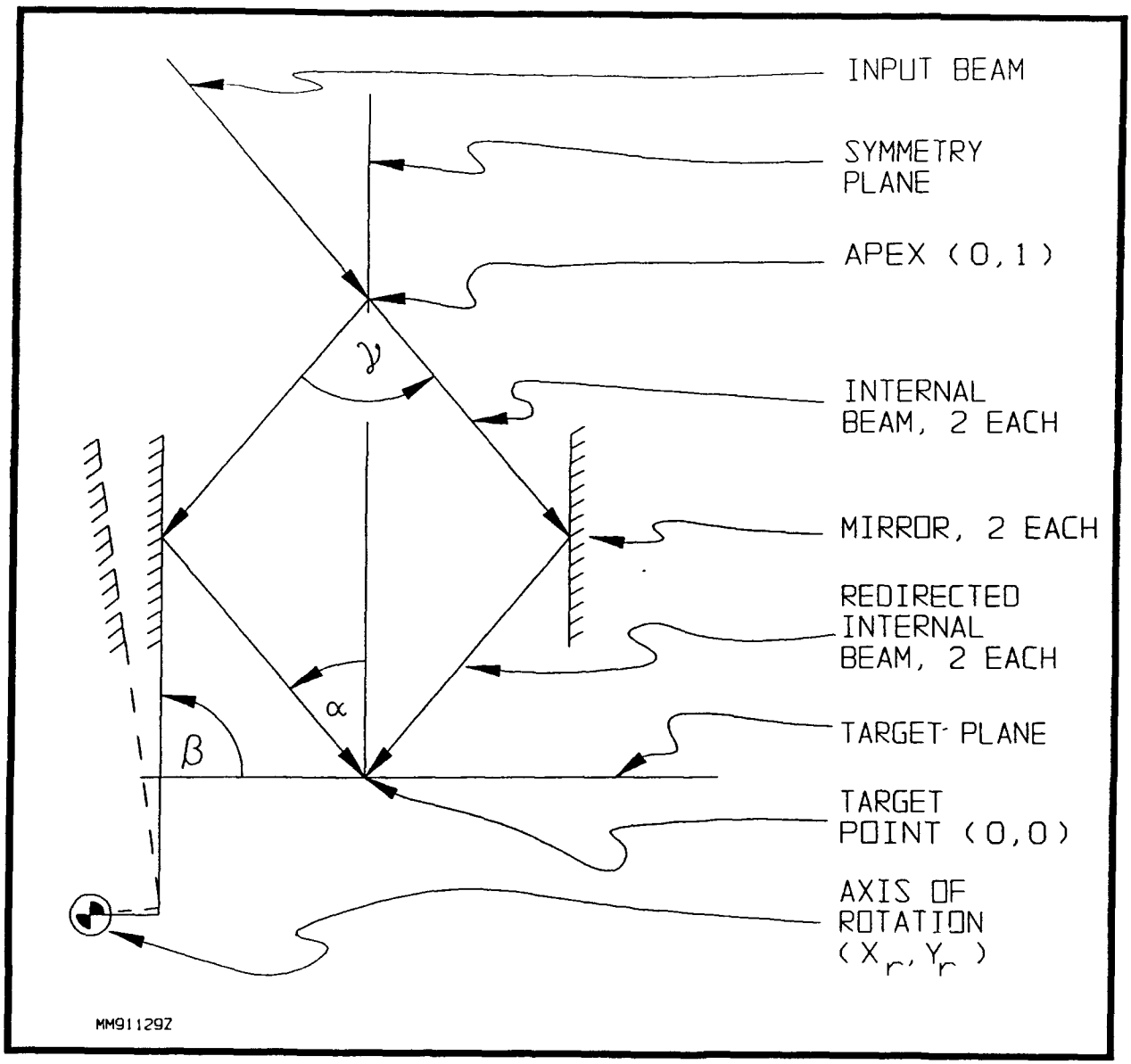

Fig. 91 Diagram of the concept of the grating facility shown in the reference plane, see text for details. In the lower left corner the axis of rotation is shown with a connection (starting horizontal, continuing vertical in the mirror plane) to the mirror. In dashed lines a rotated and effectively translated (with respect to the internal beam) position of the mirror is indicated.

intercept the internal beams at the appropriate position in order to have the redirected internal beams hit the target point.

This claim comprises the geometric structure of a mechanical set up, which utilizes only **one axis of rotation for each mirror mount to provide the desired rotation and to a very good approximation the required simultaneous translation.** This is accomplished by optimizing the position of the axis of rotation. The principle geometry is shown in **Figure 91.**

To obtain the grating period l by using light of wavelength λ in a medium of index of refraction n the required angle α is given by

$$\alpha = \alpha(\lambda, n, l) = \text{arc sin}(\lambda/(2nl))$$

which implies

$$\beta = \beta(\gamma, \lambda, n, l) = 90° + \text{arc sin}(\lambda/(2nl))/2 - \gamma/4.$$

This angle defines the grating spacing; to get best definition, the two redirected internal beams should meet as closely as possible to the target point. This is facilitated by translating the mirror such that its intersection with the internal beam lets the redirected internal beam hit the target point.

The relevant geometry is fundamentally expressed by three straight lines in normalized coordinates (lower case

characters) such that the target point is at (0,0) and the apex is at (0,1): the left internal beam is $y = 1 + x \text{ cotan } (\gamma/2)$ and the left ideal redirected internal beam is $y = -x \text{ cotan } (\alpha)$. Consequently the intersection is given by

$$(x_c, y_c) = \left(\frac{-1}{\text{cotan}\left(\frac{\gamma}{2}\right) + \text{cotan}(\alpha)}, \frac{1}{1 + \frac{\text{cotan}\left(\frac{\gamma}{2}\right)}{\text{cotan}(\alpha)}} \right)$$

and the ideal mirror plane is

$$x = x_c - y_c \text{ cotan } (\beta) + y \text{ cotan } (\beta)$$

The coordinates for the mirror planes are expressed $x = x(y)$ because for $\beta = 90°$ the conventual expression $y = y(x)$ does not exist.

If the axis of rotation of the mirror mount is positioned at (x_r, y_r) and for the angle $\beta = 90°$ the position of the corresponding left mirror is x_m, then the mirror plain is

$$x = x_m + (1 - \sin(\beta))(x_r - x_m) - [y_r + \cos(\beta)(x_r - x_m)] \tan(\beta - 90°)$$

in general.

A heuristic variation of the parameters γ, D, x_m, x_r, y_r was performed utilizing numerical computation and graphic output of an error function expressing the position of incidence at the target plane as a function of l and optimized parameters were found within geometrical constraints for l = 2000 Å to l = 3000 Å. The parameters chosen for the prototype are: $\lambda = 325$ nm, $n = 1.0$, $\gamma = 90°$, and $D = 120$ mm. Then the

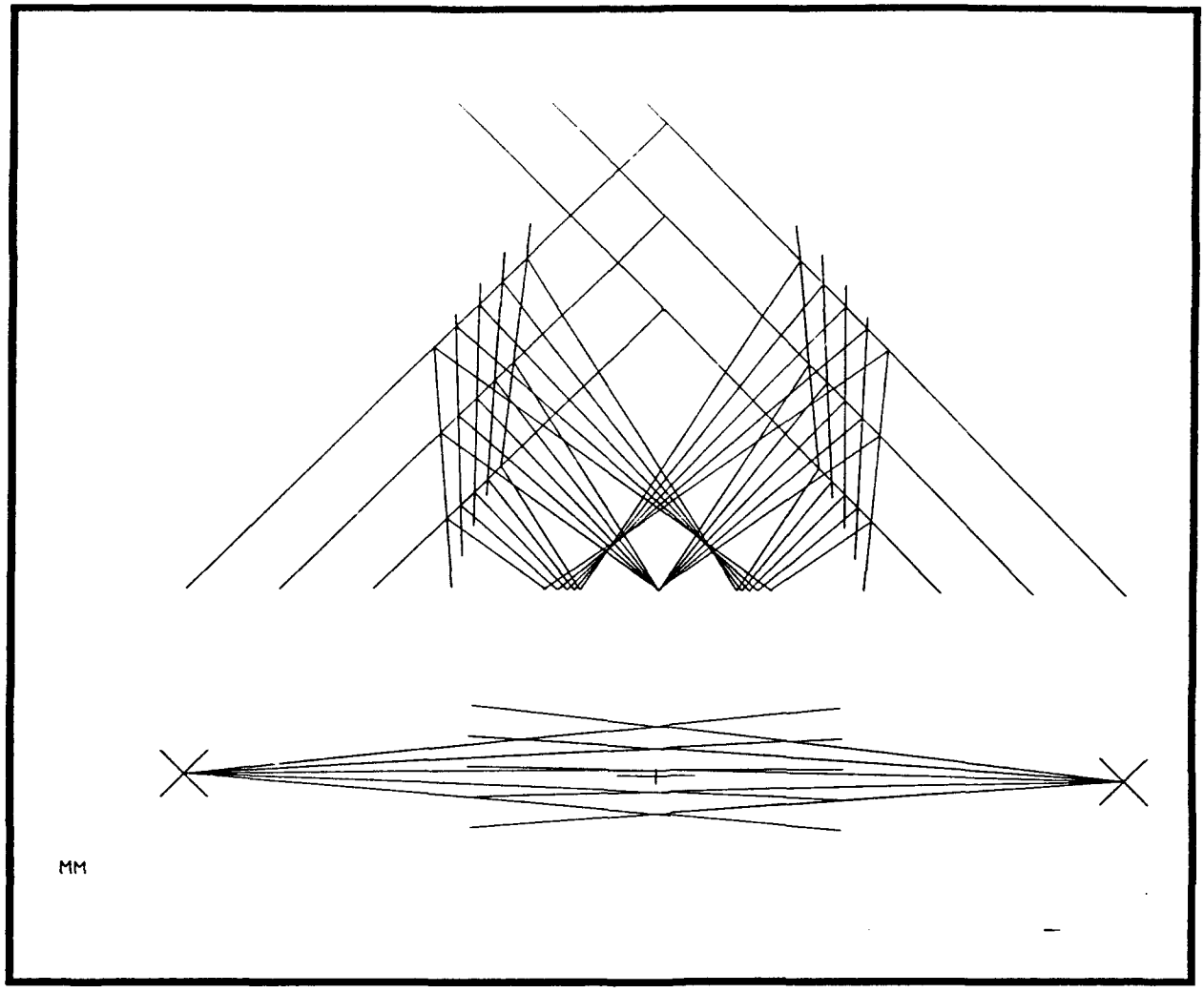

Fig. 92 Scale drawing of the geometry of the grating facility in the reference plane. Five positions of the mirrors are shown spanning the range of this design. The beam is indicated by its central ray and its outermost rays. The internal beams are continued through the mirrors. The lower part of the drawing shows the axis of rotation (large diagonal crosses) and the initially horizontal part of the L-shaped mirror mount; note the cross over because the left mirror is hinged on the right hand side and vice versa.

following values where determined (upper case characters for absolute coordinates): $X_m = -60$ mm , $X_r = +90$ mm , $Y_r = -59.52$ mm . These results show that the **optimized position of the axis of rotation for the left hand side mirror ($X_m = -60$ mm) is on the right hand side ($X_r = +90$ mm); consequently the mechanical implementation in the prototype involves crossing mirror mounts** of L-shape to clear the target area. The frame for the left and right mirror are vertically interlaced for clearance. A single translation stage positioned in the symmetry plane is used to convert a precisely controlled linear motion via two push rods to the two symmetric rotations. The fixed spacing D allows for fixed positions of the beam splitter and the target holder. Consequently a base plate is used that carries the beam splitter fixture, the target holder, and the rotary bearings for the mirror mounts as well as the translation stage to control the rotations. The angle of incidence of the redirecting mirrors of $\beta = 83.9°$ leads to $l = 3000$ Å and $\beta = 94.7°$ leads to $l = 1999$ Å . The **positioning error is within 0.017** mm **over $l = 2240$ Å to $l = 3000$ Å** and increases to 0.48 mm at $l = 1999$ Å . The set up uses **optics for 48** mm **beam diameter for large area grating definition.** The geometry is shown in the scale drawing **Figure 92.**

9.5 Operation of improved Grating Facility

A grating facility has been design and build according to the concept outlined above. This fabrication equipment has been **utilized for all the grating production that occurred for this research and development effort.** Gratings up to nearly one square inch in size have been fabricated successfully even so larger gratings seam to be possible. The single point adjustment of the grating period has been used to change grating periods for test structures and laser structures. It has been proven to provide a_reproducible holographic grating fabrication over an extended range of grating periods.

10 TEST STATION

A laser test station specifically for the measurement of vertical emission was design and build for this research and development effort. In chapter eight measurements taken with this instrument are described.

10.0 Abstract

The requirements, design criteria and design and use of a test station for vertically emitting lasers is described.

10.1 Requirements for Test Station

The specific requirement for a vertical emitting distributed Bragg reflector laser test station are sufficiently different to warrant and in some cases make necessary specialized equipment.

First and foremost, the emission emerges vertically with respect to the wafer plane. In order to facilitate chip-level testing, horizontal chip positioning is preferential, resulting in a **detector orientation not compatible with conventional edge emitters.** The expected vertical beam out of a second order Bragg reflector is dimensionally about two orders of magnitude larger in the longitudinal direction of the laser, the direction which replaces the transverse direction of the edge emitting

laser. If single mode operation is obtained, the **far field angle is consequently reduced by two orders of magnitude.** In order to determine the beam quality, significantly increased **resolution in the far field angle** is required.

The distance at which the far field approximation can be applied to the direct output beam is increased to the point, that it is more appropriate to use an optical system to generate an image of the far field pattern at a closer distance. The nature of the emitting area of vertical emitting Bragg reflector lasers is more complex than that of an edge emitting laser. Consequently, **multiple scans rather than only one lateral and one transverse scan may be required to map the characteristics of the far field pattern.**

The near field intensity distribution particular in the longitudinal direction of the laser is a signature of the grating performance. A field of view covering the length of the grating is beneficial for ease of evaluation and stage design. Visual inspection of the device under test in order to evaluate their associate near and far field results with possible material of processing inefficiencies is very desirable. It also aids in alignment.

10.2 Design of Test Station

A mechanical arrangement was conceived with two rotary stages on an ''L''-bracket such that the respective axis of rotation meet at the locus of observation at 90° with respect to each other.

The first stage with a vertical axis of rotation allows to choose the orientation of the scan or provide the scan in a horizontal plane. The second stage with a horizontal axis of rotation which is rotated by the first stage allows to scan in the vertical plane. The view of the device and the test is via the 5 X or 40 X long working distance objective or near field photodiode or far field imaging lens. The detection is via a far field photodiode or an eyepiece. Future extensions could include a CCD camera. These options are chosen by **two mechanical rotation stages** as they are used on microscopes to select objectives.

A separate XYZ-stage is utilized to position the laser in the locus of observation. The long working distance objectives are used to view the positioning process in the X- and Y- and focus in the Z-direction. The laser fixture is mounted on a thermo-electric heater/cooler for temperature control. A temperature dependent current source is used to measure the

temperature of the laser mount. A needle type probe on its own XYZ-stage is used to establish contact for the drive current of the laser.

The commercial semiconductor laser driver is utilized to control the continues current of the laser and drive the thermo-electric heater/cooler. It is equipped with the GPIB for computer interconnect. A commercial controller card for the rotary stages is inserted into an IBM XT computer for control of the scans. A custom made interface and motor power driver integrates all the components to provide coordinated operation as well as test and alignment facilities to the laser test system.

11 MATERIAL INVESTIGATION

Due to concern about observed short lifetimes of laser for this research and development effort some material investigations where included.

11.0 Abstract

Degradation of test lasers of broad stripe geometry was evaluated.

11.1 Single Quantum Well Material Investigation

We have observed that the broad area lasers we use for material characterization degrade significantly in the course of several hours of CW operation. The more complicated structures utilized to perform for the special properties considered in this contract only mask the underlying problem of the material. Consequently, investigations on the properties of our single quantum well structures were started on broad area lasers. The degradation appeared primarily in the CW light verses current curvē (L-I) as well as to a lesser degree in the pulsed L-I . Increased device heating could cause this behavior, so thermal impedance and contact resistance were investigated as possible causes. Experiments were performed to improve the contacts. As a result, the p-contact metal thickness was changed to now use a 200 Å Cr layer followed by and mediated second evaporation of 2500

Å Au. Also a new cleaning procedure was instituted before p-contact metallization. Contact resistance was measured to be 300 Ohm per square micrometer. With persisting degradation, attention was given to electron induced current (EBIC) measurements. Also lasers were operated for extended time just below threshold to current stress them but eliminate optical damage. On the other hand, devices were stored at high temperature and no degradation was found. In conclusion, the problem seemed to be either current or electric-field induced.

Experiments on the degradation of single quantum well lasers of the oxide stripe type were continued. The efforts focused on the possibility that strain due to the SiO_2-semiconductor interface was accelerating the aging of the devices. To explore this hypothesis, one set of lasers was fabricated with a 1000 Å thick SiO_2 and another set with a 2500 Å thick SiO_2 layer. Lasers were mounted, characterized and operated at constant current at a heat sink temperature of 80-90°C . Then they were re-characterized at regular intervals. The degradation rate for both groups of devices was similar.

In an attempt to reduce the strain further, lasers were fabricated with an n-type blocking layer on top of the regular cladding layer. These devices do not employ any SiO_2 layer but rely on an additional n-type GaAs layer creating a reverse biased p-n-junction. In the region in which current is to be

injected, the n-type blocking layer is etched away. As a control, the n-type blocking layer was completely removed on one piece of the wafer, and standard oxide stripe lasers were fabricated. Eight of the n-type blocking layer and eight of the control devices were subjected to the above introduced constant current 80-90°C heat sink temperature burn in procedure. Both groups showed the same degradation rate. More of these lasers will be burned in to develop better statistics.

12 FIGURE CAPTIONS

Fig. 11 Concept of implementing optical interconnects in intra computer and network application.

Fig. 12 Detail of monitor photo diode (PD), Feedback Bias Control, Duty Cycle Detector, and Current Summing ($\sum$) components required for proper operation of conventional semiconductor laser operation in an optical interconnect. This complexity stimulates considerations about direct drive no lasing bias operations of optical interconnect lasers.

Fig. 13 Concept of implementation of extra cavity folding mirror in a monolithic vertical emitting laser.

Fig. 14 Concept of implementation of intra cavity folding mirror in a monolithic vertical emitting laser.

Fig. 15 Vertical short cavity, vertically emitting laser utilizing multiple active regions here shown with conventional mirrors.

Fig. 16 Conventional double cleaved lasers (top) half ring lasers (middle) and full ring lasers (bottom) integrated in a large scale integrated opto-electronic circuit. Not the restriction on the chip size due to the resonator size in the conventional case. In the case of full ring lasers all restrictions on the placement of the lasers within the integrated circuit have been removed.

Fig. 21 Single quantum well layer structure[10]. On the left, the profile of the Al-concentration is illustrated as well as the approximate index of refraction of the material.

Fig. 22 Calculated modal gain vs. pump current density[5]. The upper trace applies for the single quantum well structure shown in Figure 21 the lower right trace applies to a conventional double heterostructure laser.

Fig. 23 Structure of the buried heterostructure single quantum well laser.

Fig. 24 Pulse response of 0.95 mA threshold quantum well laser. At the top a typical drive current pulse. At the bottom (inverted scale) light output response at peak currents of 7.4, 10.8, 16.8, 23 and 30 mA [2].

Fig. 25 Measured delay of laser output light in response to drive current pulse as a function of threshold to pulse current ratio. The absolute time reference for the delay measurement is obtained by fitting to a calculation based on a 2 ns average lifetime of the carriers at threshold.

Fig. 26 Schematic of pulse response of proposed laser structure. Driven with 15 mA current pulses from an idle current of 0.15 mA (non-lasing) a pattern effect not exceeding 20 ps is expected.

Fig. 31 Perspective drawing of proposed ring laser structure. The elongated ring in the middle of the semiconductor chip is shown with a trench etched down to a surface grating from which the output beam emerges vertically.

Fig. 32 Schema of layer-structure used for buried single quantum well lasers. The Aluminium concentration as a function of position in the grown material is shown vertically and the approximate index of refraction at the lasing wavelength is indicated.

Fig. 33 Ridge wave-guide structure. The cross-section is evident to the lower left hand side while the non-planar surface is shown to the upper right.

Fig. 51 Schematic view of the 180° curved wave-guide buried heterostructure single quantum-well graded index separate confinement heterostructure laser which utilizes a single facet. The two output beams emerge to the lower left, the facet shows the buried structure and the top shows the half-ring shape of the wave-guide.

Fig. 52 The light output versus pump current input characteristic of the coated half-ring lasers operated cw with radii of curvature of 150 μm and 100 μm. The marks at 41 mA, 29 mA, and 40 mA respectively indicate the bias points for the high frequency response measurements.

Fig. 61 The light output versus pump current input characteristic of the coated half-ring lasers operated cw with radii of curvature of 150 μm. The threshold is 6.8 mA and the slope efficiency is 0.33 W A^{-1} when light from both ends is measured.

Fig. 62 Schematic diagram of the staircase like density of states as a function of energy. The shading indicates the occupation and the lower set of curves gives the associated spectral gain distribution. While (a) describes a moderate peak gain situation, (b) describes the case of high required gain and the maximum gain is obtained from the second quantized state.[1] The high occupation of states providing the wide gain spectrum is causing the threshold current density to be high in this case.

Fig. 71 Cross-sections of ring ridge wave-guide test structure scaled to 12.500 X magnification as taken from SEM pictures. The [0 $\bar{1}$ 1] at the top shows the V-groove characteristic. The [0 0 1] at the middle was obtained form braking the chip. The [0 1 1] at the bottom exhibits up to 0.35 µm overhang characteristic for the dove-tail orientation.

Fig. 72 Perspective SEM view of half-ring ridge wave-guide laser. The ridge is the narrow elevated region close to the outer etch of the top metal (showing bright in the picture).

Fig. 81 SEM of etched grating (left) next to simulated active region of ring laser (right) showing the short transition region.

Fig. 82 SEM cross-section shows a grating etched near an 0.75 µm high step in the (0 1 1) orientation starting within 3 µm of the step.

Fig. 83 SEM cross-section shows a grating etched near a step of 1.8 µm height. In this case the grating starts immediately at the lower end of the slop of the step which is in the (0 $\bar{1}$ 1) orientation.

Fig. 84 SEM perspective of the end of a ridge in the ($\bar{0}$ 1 1) orientation. The grating formation is spaced 3.2 µm from the bottom of the slop as indicated by the markers. This photo shows a smooth transition of the ridge wave-guide into the grating region.

Fig. 85 SEM perspective of grating formation abruptly a the end of a ridge test structure which is orientated along the (0 $\bar{1}$ 1) direction.

Fig. 86 SEM top view of strip mesa same 5.5 μm wide and a grating with a 2500 Å period. The white line is a marker which was used to determine the grating period.

Fig. 87 SEM perspective view of a mounted vertical emitting laser. Shown as a small dark area is the grating region near the middle of the picture. The trench across the chip interrupts the metallization and exposes the grating. Two wire bonds are used to provide current to the two active regions.

Fig. 91 Diagram of the concept of the grating facility shown in the reference plane, see text for details. In the lower left corner the axis of rotation is shown with a connection (starting horizontal, continuing vertical in the mirror plane) to the mirror. In dashed lines a rotated and effectively translated (with respect to the internal beam) position of the mirror is indicated.

Fig. 92 Scale drawing of the geometry of the grating facility in the reference plane. Five positions of the mirrors are shown spanning the range of this design. The beam is indicated by its central ray and its outermost rays. The internal beams are continued through the mirrors. The lower part of the drawing shows the axis of rotation (large diagonal crosses) and the initially horizontal part of the L-shaped mirror mount; note the cross over because the left mirror is hinged on the right hand side and vice versa.